Araştırma Makalesi/Original Article
Makale Dili "İngilizce"/Article Language "English"

Türk Hijyen ve Deneysel Biyoloji Dergisi

Apoptotic effect of doxorubicin delivering micelles on MDA-MB-231 triple negative breast cancer cells

Doksorubisin taşıyan misellerin MDA-MB-231 üçlü negatif meme kanseri hücreleri üzerindeki apoptotik etkisi

Gülhan IŞIK ERTOP[1] (ID), Aysel KIZILTAY[2] (ID), Nesrin HASIRCI[3] (ID), Ayşen TEZCANER[4] (ID)

ABSTRACT

Objective: Many anticancer agents exhibit limited therapeutic efficacy due to high systemic toxicity or rapid elimination by the reticuloendothelial system. Therefore, nanocarrier systems that enable drug targeting directly to tumor tissue have become a significant research area in recent years. The aim of this study was to prepare and characterize methoxy polyethylene glycol-block-polycaprolactone (mPEG-b-PCL)-based doxorubicin (DOX)-loaded micelles (DOX_{ld}-M) and micelles formed by covalent conjugation of DOX (DOX_{conj}-M), and to compare the biological effects of these systems on MDA-MB-231 breast cancer cells.

Methods: DOX was either loaded directly onto mPEG-b-PCL micelles (DOX_{ld}-M) or covalently conjugated to hydrazide-functionalized mPEG-b-PCL (DOX_{conj}-M), resulting in micelle formation. The physicochemical properties and drug release profiles of the micelles were determined. At the cellular level, their effects

ÖZET

Amaç: Birçok antikanser ajanı, yüksek sistemik toksisite veya retiküloendotelyal sistem tarafından hızlı eliminasyon nedeniyle terapötik etkinliğini sınırlı düzeyde gösterebilmektedir. Bu nedenle, ilacın doğrudan tümör dokusuna hedeflenmesini sağlayan nano-taşıyıcı sistemler son yıllarda dikkat çekici bir araştırma alanı haline gelmiştir. Bu çalışmanın amacı, metoksi polietilen glikol-blok-polikaprolakton (mPEG-b-PCL) esaslı doksorubisin (DOX) yüklü miseller (DOX_{ld}-M) ile DOX kovalent konjugasyonu ile oluşturulan misellerin (DOX_{conj}-M) hazırlanması, karakterizasyonu ve bu sistemlerin MDA-MB-231 meme kanseri hücreleri üzerindeki biyolojik etkilerinin karşılaştırılmasıdır.

Yöntem: BDOX, ya doğrudan mPEG-b-PCL misellerine yüklenmiş (DOX_{ld}-M) ya da hidrazid fonksiyonlu mPEG-b-PCL'ye kovalent olarak bağlanarak konjuge edilmiş (DOX_{conj}-M) ve sonrasında misel yapısı oluşturulmuştur. Misellerin fizikokimyasal özellikleri ve ilaç salım profilleri belirlenmiştir. Hücresel düzeyde

[1]Health Institutes of Türkiye, Türkiye Cancer Institute, İstanbul, Türkiye
[2]Central Laboratory, Middle East Technical University, Ankara, Türkiye
[3]Department of Chemistry, Middle East Technical University, Ankara, Türkiye
[4]Department of Engineering Sciences, Middle East Technical University, Ankara, Türkiye

İletişim / Corresponding Author : Gülhan IŞIK ERTOP
Türkiye Sağlık Enstitüleri Başkanlığı, Türkiye Kanser Enstitüsü, İstanbul - Türkiye
E-posta / E-mail : glhn.isik@gmail.com

Geliş Tarihi / Received : 27.02.2025
Kabul Tarihi / Accepted : 02.10.2025

DOI ID : 10.5505/TurkHijyen.2025.29660

Işık Ertop G, Kızıltay A, Hasırcı N, Tezcaner A. Apoptotic effect of doxorubicin delivering micelles on MDA-MB-231 triple negative breast cancer cells. Turk Hij Den Biyol Derg, 2025; 82(4): 621 - 650

on cytotoxicity, cell internalization, cell migration, and colony formation were evaluated in MDA-MB-231 cells. Apoptotic responses were investigated using flow cytometry, qRT-PCR, mitochondrial transmembrane potential measurements, and reactive oxygen species (ROS) assays. Furthermore, the anti-angiogenic effects of both micelle formulations were investigated in a co-culture system with HUVEC cells.

Results: Both micelle types exhibited faster drug release under acidic conditions compared to neutral conditions, offering a therapeutic advantage given the acidic nature of the tumor microenvironment. DOX conjugation provided more controlled and slower drug release compared to loading. Drug-free micelles did not exhibit any cytotoxicity. The natural fluorescence of DOX confirmed that the micelles were effectively internalized by the cells. All DOX-containing micelles significantly suppressed proliferation and migration in MDA-MB-231 cells. In particular, DOX_{ld}-M was characterized by an increase in the proportion of apoptotic cells, a significant increase in Bax and p53 gene expression, a significant decrease in Bcl-2 and Bcl-xL expression, and an increase in ROS production. Both micelle formulations decreased mitochondrial membrane potential and triggered apoptosis induction.

Conclusion: The results indicate that DOX_{ld}-M was more effective than DOX_{conj}-M in inducing apoptosis and inhibiting proliferation of MDA-MB-231 cells. These findings suggest that mPEG-b-PCL-based DOX-loaded micelles may be promising nanocarrier systems for cancer therapy.

Key Words: Doxorubicin, hydrazone, drug loading, breast cancer, apoptosis

ise, MDA-MB-231 hücrelerinde sitotoksisite, hücre içine alımı, hücre göçü ve koloni oluşumu üzerine etkileri değerlendirilmiştir. Apoptotik yanıtlar; akış sitometrisi, qRT-PCR, mitokondriyal transmembran potansiyel ölçümleri ve reaktif oksijen türleri (ROS) tayini ile incelenmiştir. Ayrıca, HUVEC hücreleriyle yapılan ko-kültür sisteminde her iki misel formülasyonunun anti-anjiyogenik etkileri araştırılmıştır.

Bulgular: Her iki misel türü de asidik koşullarda nötr ortama kıyasla daha hızlı ilaç salımı göstermiş olup bu durum, tümör mikroçevresinin asidik karakteri açısından terapötik avantaj sunmaktadır. DOX konjugasyonu, yüklemeye kıyasla daha kontrollü ve yavaş ilaç salımı sağlamıştır. İlaç içermeyen miseller herhangi bir sitotoksisite göstermemiştir. DOX'un doğal floresansı, misellerin hücreler tarafından etkin biçimde internalize edildiğini doğrulamıştır. Tüm DOX içeren miseller MDA-MB-231 hücrelerinde proliferasyon ve göçü belirgin şekilde baskılamıştır. Özellikle DOX_{ld}-M, apoptotik hücre oranında artış, Bax ve p53 gen ifadesinde belirgin yükseliş, Bcl-2 ve Bcl-xL ifadesinde anlamlı azalma ve ROS üretiminde artış ile karakterize edilmiştir. Her iki misel formülasyonu da mitokondriyal membran potansiyelinde azalmaya yol açmış ve apoptoz indüksiyonunu tetiklemiştir.

Sonuç: Sonuçlar, DOX_{ld}-M'nin apoptoz indüklemede ve MDA-MB-231 hücrelerinin proliferasyonunu engellemede DOX_{conj}-M'ye kıyasla daha etkili olduğunu göstermektedir. Bu bulgular, mPEG-b-PCL tabanlı DOX yüklü misellerin kanser tedavisinde umut vadeden nano-taşıyıcı sistemler olabileceğini ortaya koymaktadır.

Anahtar Kelimeler: Doksorubisin, hidrazon, ilaç yükleme, meme kanseri, apoptoz

INTRODUCTION

Breast cancer is the most common cancer type in women, and approximately 20% of these patients present with metastasis. It is the second leading cause of cancer-related death after lung cancer (1). Breast cancer is classified into several subtypes, including estrogen receptor-positive breast cancer (ERBC), progesterone receptor-positive breast cancer (PRBC), human epidermal growth factor receptor 2-positive

breast cancer (HER2-BC) and triple negative breast cancer (TNBC). TNBC accounts for about 20% of all breast cancers, which lacks a cell surface receptor and is highly aggressive. Due to the absence of targetable receptors, cancer-targeted drug delivery systems are generally ineffective against this subtype (2). Moreover, TNBC exhibits resistant to radiotherapy, making its treatment particularly challenging (3).

Anthracycline antibiotics are commonly used in cancer treatment. These agents act as alkylating agents, intercalate into DNA, inhibit topoisomerase activity, and generate free radicals, thereby causing oxidative damage to cellular proteins. Doxorubicin (DOX), a widely used anthracycline antibiotic, binds directly to DNA, induces single- and double-strand breaks, and can crosslinks DNA. DNA. However, its clinical use is limited by dose-dependent cardiotoxicity (4).

Cancer cells preferentially utilize glycolysis over oxidative phosphorylation to meet the high energy demand required for rapid proliferation. This metabolic shift leads to hypoxia within the tumor microenvironment, causing pH values to decrease to 6.5-7.2 in the extracellular space, 5.0-6.5 in endosomes, and 4.5-5.0 in lysosomes (5). pH sensitive drug delivery systems, typically exploit this feature by linking drugs to polymers through pH-responsive linkers such as hydrazone, disulfide, azo, acetal, ortho ester, vinyl ether, amine, or imine bonds (6). Hydrazone linkages are particularly promising, as they remain stable under physiological conditions (pH 7.4) but are cleaved in acidic environments (7). For instance, Etrych et al. (2014) conjugated DOX to N-(2-hydroxypropyl)methacrylamide (HPMA) copolymers via hydrazone bonds and reported faster drug release at pH 5.0 compared to pH 7.4 (8). Similarly, Lale et al. (2015) demonstrated that DOX conjugated to a pentablock copolymer via hydrazone bonds released 89% of the drug at pH 5.0, whereas only 29% was released at pH 7.4 (9). More recently, Zhang et al. (2022) conjugated DOX to a supramolecular organic framework via hydrazone bonds, reporting DOX release levels of 80%, 45%, and 15% at pH 4.5, 5.6, and 7.4, respectively, after 72 hours. The amounts of the released DOX were 80%, 45% and 15% at pH 4.5, 5.6 and 7.4, respectively after 72 hours (10). Collectively, these findings confirm that hydrazone linkages are pH-responsive, enabling accelerated drug release under acidic conditions compared to physiological environments.

Polymeric micelles are nano-sized particles composed of a hydrophilic shell and a hydrophobic core in aqueous media. Hydrophobic anticancer drugs can be encapsulated within the hydrophobic core, thereby improving drug bioavailability, reducing systemic side effects, and offering advantages in both in vitro and in vivo studies (11–14). These systems are relatively easy to prepare, can be synthesized with small and uniform particle sizes, and provide high drug-loading capacity as well as controlled drug release. Methoxy poly(ethylene glycol)-block-polycaprolactone (mPEG-b-PCL) is a synthetic, amphiphilic, biocompatible and biodegradable polymer approved by FDA (15). Poly(ethylene glycol) (PEG) and polycaprolactone (PCL) are biocompatible polymers which are widely used in drug delivery systems and tissue engineering (16). However, PCL's highly hydrophobic nature, slow degradation rate, and immunogenicity limit its application (17). On the other hand, PEG is hydrophilic and helps nanoparticles evade immune recognition. Therefore, di-block or tri-block copolymers of PEG and PCL have been developed to produce nanoparticles or micelles, which have shown promising in vitro and in vivo results as drug delivery systems (18–21).

The aim of the present study was to prepare DOX-loaded and DOX-conjugated mPEG-b-PCL micelles and compare their anticancer effects on MDA-MB-231 breast cancer cells. To develop pH responsive controlled delivery systems, DOX-conjugated micelles (DOX_{conj}-M) were synthesized using hydrazide-functionalized mPEG-b-PCL, which was covalently linked to DOX via pH-sensitive hydrazone bonds. In parallel, DOX-loaded micelles (DOX_{ld}-M) were prepared using unmodified PEG-b-PCL copolymer. The

physicochemical properties of the micelles, as well as their cytotoxic and apoptotic effects on MDA-MB-231 cells, were systematically evaluated and compared.

MATERIAL and METHOD

Materials

Adriamycin (trade name of DOX) was purchased from Deva Holding (Turkey) as lyophilized powder of 10 mg of Doxorubicin hydrochloride in injection vials. ε-caprolactone (ε-CL) was purchased from Acros Organics, USA. Methoxy poly(ethylene glycol) (mPEG) (Mn=5000 Da), tin(II) 2-ethylhexanoate, succinic anhydride, dimethylaminopyridine, dicyclohexylcarbodiimide, N-hydroxysuccinimide, hydrazine hydrate, glycine, sodium bicarbonate, trinitrobenzene sulfonic acid (TNBSA), polyvinyl alcohol, 3-(4,5-dimethylthiazol-2-yl)-2,5-diphenyltetrazolium bromide (MTT), dimethylsulfoxide (DMSO), paraformaldehyde, crystal violet, and oil red O were the products of Sigma-Aldrich, Germany. Tetrahydrofuran, diethyl ether, methanol, trifluoroacetic acid, concentrated sulfuric acid, acetone, and ethanol were purchased from Merck, Germany. Leibovitz's L-15 medium, fetal bovine serum (FBS), gentamicin, and penicillin-streptomycin were the products of Biological Industries, Israel.

Methods

Synthesis and Characterization of Hydrazide Functionalized mPEG-b-PCL Copolymer (mPEG-b-PCL-CO-NH-NH_2)

mPEG-b-PCL copolymer was synthesized by ring-opening polymerization of ε-caprolactone (CL) according to the method previously reported by our group (22). In our previous study, the hydrazide functionalized copolymer was synthesized in two steps (23):

1. Introduction of a carboxylic acid group at the PCL end of the copolymer using succinic anhydride in the presence of dimethylaminopyridine (DMAP) and tetrahydrofuran (THF).

2. Subsequent incorporation of the hydrazide group at the terminal carboxylic acid moiety using dicyclohexylcarbodiimide (DCC), N-hydroxysuccinimide (NHS), and THF.

The synthesized copolymer was characterized with ^{1}H NMR, and FT-IR. The primary amine amount was calculated with trinitrobenzene sulfonic acid assay as previously described (23).

Conjugation of DOX to mPEG-b-PCL-CO-NH-NH_2

DOX was conjugated to mPEG-b-PCL-CO-NH-NH_2 following the method reported by our group (23). Briefly, both mPEG-b-PCL-CO-NH-NH_2 copolymer and DOX were dissolved in methanol, a drop of TFA was added, and the solution was incubated overnight at 60°C. After methanol removal under vacuum, the residue was suspended in water and dialyzed against deionized water at RT. The DOX-conjugated copolymer (mPEG-b-PLC-CO-NH-NH_2-DOX) was obtained after lyophilization. Conjugation efficiency was calculated using a calibration curve constructed for DOX, following its dissolution in concentrated sulfuric acid at RT for 5 min (23).

Critical Micelle Concentration (CMC) of DOX Conjugated mPEG-b-PCL-CO-NH-NH_2

The CMC of DOX-conjugated copolymers was determined using pyrene as a fluorescent probe. For this purpose, 20 mg of polymer was dissolved in 5 mL of THF, followed by the addition of 40 mL of deionized water. The solution was left in a fume hood for THF evaporation. Pyrene solutions of varying concentrations ($0.5x10^{-3}$ - 0.5 g/L) in 0.6 mM acetone were prepared. Subsequently, 10 µL of pyrene solutions were added to 1 mL of polymer solutions and the mixtures were incubated at 37°C overnight. Excitation spectra were recorded between 250-360 nm at a fixed emission wavelength of 390 nm with a 1 nm bandwidth using a microplate reader. The intensity ratio at 338 and 333 nm (I_{338}/I_{333}) was plotted

against the logarithm of polymer concentrations. CMC was determined from the intersection of the two tangent plots (24).

Preparation of DOX Conjugated (DOX_{conj}-M) and DOX Loaded (DOX_{ld}-M) Micelles

Micelles were prepared using co-solvent evaporation method (25). For DOX_{conj}-M, 30 mg of mPEG-b-PCL-CO-NH-NH_2-DOX copolymer was dissolved in 0.5 mL of acetone. For DOX_{ld}-M, 30 mg of mPEG-b-PCL-CO-NH-NH_2 copolymer and 3 mg of DOX were dissolved in 0.5 mL of acetone containing 5 µL of triethylamine. To each solution, 3 mL of 1% PVA was added dropwise under vigorous agitation. The resulting micelle suspensions were mixed at 1100 rpm for 5 h to allow solvent evaporation and micelle formation. Micelles were collected by centrifugation at 14,000 rpm for 20 min at 4°C. For purification, micelles were washed twice by resuspension in distilled water and centrifugation. The final micelles were suspended in 5 mL of distilled water, passed through a 0.22 µm syringe filter, and freeze-dried (FreeZone 6 Plus, Labconco Corp., USA) for 24 h before storage in dry form. Before freeze-drying, the hydrodynamic diameter and zeta potential of these micelles (M) (having no drugs) were determined using a Malvern Zetasizer Nano ZS (Malvern Instruments Ltd., MA). All measurements were performed in triplicates (n=3) to ensure reproducibility.

Encapsulation efficiency and drug loading capacity of DOX_{conj}-M and DOX_{ld}-M were calculated using the equations given below. Briefly, weighed amounts of freeze-dried micelles were dissolved in concentrated sulfuric acid, and DOX absorbance was measured at 543 nm using a UV-visible spectrophotometer (Hitachi U-2800A, Hitachi Ltd., Japan). DOX content was quantified using the previously established calibration curve (23). Blank micelles (without DOX) dissolved in concentrated sulfuric acid were used as background controls. All measurements were performed in triplicates (n=3) to ensure reproducibility.

$$Encapsulation\ efficiency\ (\%) = \frac{(The\ amount\ of\ drug\ inside\ the\ micelles)}{(The\ initial\ amount\ of\ drug\ added)} \times 100$$

$$Drug\ loading\ capacity\ (\%) = \frac{(The\ amount\ of\ drug\ inside\ the\ micelles)}{(The\ amount\ of\ micelles)} \times 100$$

Release of DOX from DOX_{conj}-M or DOX_{ld}-M

The release of DOX from DOX_{conj}-M or DOX_{ld}-M micelles was evaluated in three different media with pH values of 7.4, 6.8 and 5.0. For this study, 10 mg of DOX_{conj}-M or DOX_{ld}-M was suspended in 1 mL of phosphate-buffered saline (PBS, 0.1 M and pH 7.4) or 1 mL of citrate-phosphate buffer (CPB, 0.15 M; pH 5.0 or pH 6.8) (n = 6). Free DOX was dispersed in PBS-7.4 or CPB-5.0 or CPB-6.8 (1 mg DOX/ mL) and used as control groups. Micelle solutions and free DOX solutions were transferred into dialysis bags (MWCO is 3500 Da; Spectrum Laboratories, USA), placed in 4 mL of the corresponding release medium, and incubated in a thermostatic shaker (37°C, 80 rpm) (Nüve ST-30, Türkiye). At predetermined intervals, 2 mL of the release media was withdrawn and replaced with fresh buffer. Collected samples were freeze-dried, dissolved in ethanol, and analyzed using a microplate reader (SpectraMax iD3, Molecular Devices, USA) at an excitation wavelength of 480 nm and an emission wavelength of 590 nm. The amount of DOX in the release medium was quantified using a calibration curve constructed from DOX solutions in ethanol. To investigate the release mechanism, the data were fitted to zero order (cumulative percent release of DOX versus time plot), first order (log cumulative percent of DOX remaining versus time plot), Higuchi model (cumulative percent of DOX release versus square root of time plot), and Korsmeyer-Peppas (log cumulative percent release of DOX versus log time plot) kinetic models.

In Vitro Cell Culture Experiments

Determination of IC_{50} of DOX on MDA-MB-231 Cells

The cytotoxic effect of different concentrations of DOX on MDA-MB-231 triple negative breast cancer cells

was evaluated to determine the IC_{50} value. Cells were cultured in Leibovitz's L-15 medium supplemented with 15% FBS, 0.1% gentamicin and 0.1% penicillin-streptomycin at 37°C in a 5% CO_2 atmosphere. Then, cells were seeded in 96-well plates at a density of 2500 cells/well in 100 µL medium and allowed to adhere overnight. The following day, the medium was replaced with fresh medium containing DOX at concentrations ranging from 0 nM to 90 nM (prepared from 400 µM DOX stock solution) in 0.4% water, and cells were incubated for 48 hours. Subsequently, 10 µL of MTT solution (5 mg/mL) was added to each well., cells treated with 0.4% water-containing medium were used as the negative control. After 4 h of incubation, the solutions were discarded, and the formazan crystals were solubilized in 50 µL DMSO for 20 min on an orbital shaker. The solutions were then transferred to a new 96-well plate, and absorbance was measured at 570 nm (SpectraMax iD3, Molecular Devices, USA). Cell viability was calculated as the percentage of the negative control, and the IC50 value was calculated using GraphPad Prism 8 (GraphPad Software, USA) (n=4).

Cytotoxicity of DOX_{conj}-M and DOX_{ld}-M on MDA-MB-231 Cells

MDA-MB-231 triple negative breast cancer cells treated with DOX_{conj}-M, or DOX_{ld}-M were incubated at 37°C in 5% CO2 atmosphere to compare their cytotoxic effects. Empty micelles without any drug (M) were also used to show cytocompatibility. Cells were seeded in 96-well plates at a density of 2500 cells/well in 100 µL medium and allowed to adhere overnight. The next day, the medium was replaced with fresh medium containing micelles (1.5 mg/mL) dispersed in complete medium. Free DOX containing medium was used to check the effectiveness of micelles compared to free drug. Cytotoxicity was evaluated by MTT assay, as described previously. Cells incubated in pure medium served as positive controls and were considered 100% viable (n=4).

Determination of Cell Internalization of Micelles

The intrinsic fluorescence of DOX was used to assess the internalization of free DOX, DOX_{conj}-M, and DOX_{ld}-M in MDA-MB-231 cells. Cells were seeded on coverslips at a density of 1x105 cells/well in 1 mL medium and allowed to adhere overnight. The next day, the medium was replaced with fresh medium containing free DOX (80 nM), DOX_{conj}-M (1.5 mg/mL), or DOX_{ld}-M (1.5 mg/mL) in complete medium. Samples were incubated for 1, 2, 4 and 6 h at 37ºC. At each time point, cells were washed with cold PBS, fixed with 4% paraformaldehyde (w/v) at RT, and stained with DAPI. Internalization was observed by confocal microscopy (Zeiss Cell Observer SD, Germany).

Cell Migration Assay

Cell migration was assessed using transwell chambers for 24-well plates with 8.0 µm pores (Greiner, Austria) (26). MDA-MB-231 cells were seeded in the inserts at a density of $6x10^4$ cells/insert in 200 µL of serum-free medium containing free DOX (80 nM), M (1.5 mg/mL), DOX_{conj}-M (1.5 mg/mL), or DOX_{ld}-M (1.5 mg/mL). Untreated cells were used as the control group. The lower chambers were filled with 500 µL serum containing medium. After 48 h, non-migrated cells were removed with a cotton swab, while migrated cells were fixed with 4% paraformaldehyde (w/v) and stained with 0.2% crystal violet (w/v). Chambers were washed with water and left to dry. Images were acquired using an inverted phase-contrast microscope (Nikon Eclipse TS100, Nikon Corp, USA), and migrated cells were quantified in three random fields using ImageJ software. The percentage of migrated cells was normalized with respect to the control (n=3).

Colony Formation Assay

Colony formation was evaluated after treatment with M, DOX_{conj}-M, or DOX_{ld}-M. MDA-MB-231 cells were seeded in 6-well plates at a density of 2000 cells/well and cultured for 24 h. Then, cells were treated with free DOX (80 nM), M (1.5 mg/mL), DOX_{conj}-M (1.5 mg/

mL), or DOX_{ld}-M (1.5 mg/mL) for one week. Thereafter, colonies were fixed with 4% paraformaldehyde (w/v) for 20 min, stained with 0.2% crystal violet (w/v), and counted manually. The experiment was performed in triplicates (n=3) (26). Untreated cells were used as controls.

Determination of Lipid Droplets in MDA-MB-231 Cells

To assess apoptosis, lipid droplet formation was evaluated in cells treated with free DOX, M, DOX_{conj}-M, or DOX_{ld}-M. Cells were seeded in 24-well plates at a density of $1x10^5$ cells/well in 1 mL medium and allowed to adhere overnight. The next day, cells were treated with free DOX (80 nM), M (1.5 mg/mL), DOX_{conj}-M (1.5 mg/mL), or DOX_{ld}-M (1.5 mg/mL) in complete medium and incubated for 48 h. Cells were then washed with PBS, and fixed with 4% paraformaldehyde (w/v) for 20 min. After removing the paraformaldehyde, fixed cells were treated with 60% isopropanol for 5 min. Lipid droplets were stained with Oil Red O for 30 min, followed by counterstaining with Weigert's hematoxylin for 10 min. Finally, cells were washed three times with water, and lipid droplets were visualized and photographed using an inverted phase-contrast microscope (Nikon Eclipse TS100, Nikon Corp, USA) (27).

Detection of Apoptosis in Cancer Cells with qRT-PCR

Apoptotic gene expression was evaluated in MDA-MB-231 cells treated with M, DOX_{conj}-M, or DOX_{ld}-M. Cells were seeded in 6-well plates at a density of $1x10^6$ cells/well in 3 mL medium and allowed to adhere overnight. The following day, cells were treated with free DOX (80 nM), M (1.5 mg/mL), DOX_{conj}-M (1.5 mg/mL), or DOX_{ld}-M (1.5 mg/mL) and incubated for 24 h. Untreated cells were used as controls. Total RNA was extracted using the Roche High Pure RNA Isolation Kit (Switzerland), and cDNA was synthesized with the Roche Transcriptor High Fidelity cDNA Synthesis Kit (Switzerland), following the manufacturer's instructions. qRT-PCR was performed using LightCycler® FastStart DNA Master SYBR Green I (Switzerland). The relative expression of pro-apoptotic (Bax, and p53) and anti-apoptotic (Bcl-2, and Bcl-xL) genes was quantified relative to the reference ß-actin gene using ΔΔCT method. All measurements were performed in triplicates (n = 3) to ensure reproducibility. Primer sequences are listed in Table 1.

Table 1. Primers used in qRT-PCR studies

Primer	Sequence
Bax F	CCCGAGAGGTCTTTTTCCGAG
Bax R	CCAGCCCATGATGGTTCTGAT
p53 F	CCTCAGCATCTTATCCGAGTGG
p53 R	TGGATGGTGGTACAGTCAGAGC
Bcl-2 F	GGTGGGGTCATGTGTGTGG
Bcl-2 R	CGGTTCAGGTACTCAGTCATCC
Bcl-xL F	GAGCTGGTGGTTGACTTTCTC
Bcl-xL R	TCCATCTCCGATTCAGTCCCT
β-*actin* F	ATGTGGCCGGAGGACTTGATT
β-*actin* R	AGTGGGGTGGCTTTTAGGATG

F: Forward primer sequence, R: Reverse primer sequence.

Determination of Cell Apoptosis with Annexin V-FITC Assay

The apoptotic effects of M, DOX_{conj}-M, and DOX_{ld}-M on MDA-MB-231 cells were evaluated using an FITC Annexin V-PI kit. Briefly, cells were seeded in 6-well plates at a density of $1x10^6$ cells/well in 3 mL of complete medium and allowed to adhere overnight. The next day, the medium was replaced with fresh medium containing free DOX (80 nM), M (1.5 mg/mL), DOX_{conj}-M (1.5 mg/mL), or DOX_{ld}-M (1.5 mg/mL) and cells were incubated for 24 h. Cells treated with DOX at its IC_{50} value (80 nM) were used as the negative control. After incubation, the medium was discarded, and cells were washed with sterile PBS (0.1 M, pH 7.4), detached using a cell scraper, and collected by centrifugation at 2000 rpm for 5 min. Cells were then stained with FITC Annexin V and propidium iodide according to FITC Annexin V-PI kit protocol (BioLegend, USA). Apoptosis analysis was performed using flow cytometry (BD Accuri C6, USA). First, cells from each group were counted and dilutions were made to obtain $1x10^6$ cells/mL for each group. Data were gated to exclude debris using unstained cell suspensions. Cells stained with Annexin V-FITC and propidium iodide were analyzed, and the proportions of live and apoptotic cells were calculated relative to the untreated control group (n=3).

Mitochondrial Transmembrane Potential Detection

Changes in mitochondrial transmembrane potential ($\Delta\Psi m$) are an early hallmark of apoptosis. To assess this, 3,3'-Dihexyloxacarbocyanine iodide (DiOC6), a membrane permeable fluorescent probe that dyes mitochondria, was used. DiOC6 selectively stains mitochondria in healthy cells; however, in apoptotic cells with disrupted mitochondrial membrane integrity, DiOC6 uptake is impaired. MDA-MB-231 cells were seeded in 6-well plates at a density of $1x10^6$ cells/well in 3 mL of medium and allowed to adhere overnight. The next day, the medium was replaced with fresh medium containing free DOX (80 nM), M (1.5 mg/mL), DOX_{conj}-M (1.5 mg/mL), or DOX_{ld}-M (1.5 mg/mL) in complete medium, and cells were incubated for 24 h. Cells treated with DOX at its IC_{50} value (80 nM) were used as the negative control. After incubation, the medium was discarded, cells were washed with sterile PBS (0.1 M, pH 7.4), detached with a cell scraper, and collected by centrifugation. Cells were then incubated with 40 nM DiOC6 for 30 min, and analyzed by flow cytometry (BD Accuri C6, USA). First, cells from each group were counted and dilutions were made to obtain $1x10^6$ cells/mL for each group. Data were gated to exclude debris using unstained cell suspensions. Loss of mitochondrial transmembrane potential was determined by a reduction in the percentage of cells in the V1-R region compared with the control group (n=3) (28).

Reactive Oxygen Species (ROS) Determination

Intracellular ROS levels, which increase during apoptosis, were determined using the Cellular ROS Assay Kit (Abcam, UK). The fluorescent probe of 2',7'-Dichlorofluorescin diacetate (DCFDA) was employed to detect ROS in cells. MDA-MB-231 cells were seeded either on coverslips in 24-well plates at a density of $1x10^5$ cells/well in 1 mL medium for confocal microscopy imaging, or in 96-well plates at a density of 2500 cells/well in 100 µL medium for ROS quantification. After overnight adhesion, cells were treated with medium containing free DOX (80 nM), M (1.5 mg/mL), DOX_{conj}-M (1.5 mg/mL), or DOX_{ld}-M (1.5 mg/mL) in complete medium for 24 h. After that, the medium was discarded, and cells were incubated with 20 µM DCFDA solution for 30 min, followed by washing with PBS. Cells on coverslips were examined with confocal microscopy (Zeiss Cell Observer SD, Germany), while fluorescence intensity in 96-well plates was measured using a microplate reader (SpectraMax iD3, Molecular Devices, USA) (n=4). Medium containing 0.4% ethanol (v/v) was used as the negative control, while tert-butyl hydroperoxide (TBHP, 50 µM for 4 h) was used as the positive control prior to DCFDA staining.

Endothelial Cell Tube Formation Assay

The anti-angiogenic effects of the micelles were investigated using an endothelial cell tube formation assay (29). Human umbilical vein endothelial cells (HUVECs) were cultured in endothelial cell (EC) medium supplemented with 10% FBS. First, 50 µL of Matrigel solution (Corning, USA) was added to 96-well plates and incubated for 30-60 min at 37°C to allow polymerization. Then, $4x10^4$ HUVECs/well and/or $4x10^4$ MDA-MB-231 cells/well were seeded onto the Matrigel. Next, 150 µL of medium containing free DOX, DOX_{conj}-M, or DOX_{ld}-M was added, and cells were incubated for 2, 4, 8, and 24 h. Images were captured at each time point using an inverted microscope (Nikon Eclipse TS100, Nikon Corp, USA), and were analyzed using ImageJ software (National Institutes of Health, Bethesda, MD, USA). The total endothelial tube lengths and number of nodes were quantified using the Angiogenesis Analyzer plugin in ImageJ software. Results were averaged from three independent experiments (n=3). The experimental groups and media compositions are summarized in Table 2.

Statistical Analysis

All data are presented as mean ± standard deviation. Results were analyzed using one-way analysis of variance (ANOVA) and Tukey's multiple comparison test.

Table 2. Groups for endothelial cell tube formation assay

Group name	Cells	Medium and treatment
Control-1	HUVEC	EC medium
Control-2	HUVEC	EC:L15 medium (1:1)
Free DOX-1	HUVEC	EC medium, free DOX
Free DOX-2	HUVEC	EC:L15 medium (1:1), free DOX
Co-culture control	HUVEC:MDA-MB-231	EC:L15 medium (1:1)
Co-culture free DOX	HUVEC:MDA-MB-231	EC:L15 medium (1:1), free DOX
HUVEC1-DM1	HUVEC	EC medium, DOX_{conj}-M
HUVEC1-DM2	HUVEC	EC medium, DOX_{ld}-M
HUVEC2-DM1	HUVEC	EC:L15 medium (1:1), DOX_{conj}-M
HUVEC2-DM2	HUVEC	EC:L15 medium (1:1), DOX_{ld}-M
HUVEC1-EM	HUVEC	EC medium, M
HUVEC2-EM	HUVEC	EC:L15 medium (1:1), M
Co-culture DM1	HUVEC:MDA-MB-231	EC:L15 medium (1:1), DOX_{conj}-M
Co-culture DM2	HUVEC:MDA-MB-231	EC:L15 medium (1:1), DOX_{ld}-M
Co-culture EM	HUVEC:MDA-MB-231	EC:L15 medium (1:1), M

RESULTS

Synthesis and Characterization of Hydrazide Functionalized mPEG-b-PCL Copolymer (mPEG-b-PCL-CO-NH-NH_2)

The synthesized copolymer was characterized with ^{1}H NMR, and FT-IR spectroscopy. The presence of primary amine groups, confirming the hydrazide functionalization of the copolymer, was detected as described previously (23). The hydrazide content of mPEG-b-PCL-CO-NH-NH_2 polymer was determined to be 45.6 mole% (100 moles of polymer contains 45.6 moles of -NH_2 as hydrazide group.) (23).

Conjugation of DOX to mPEG-b-PCL-CO-NH-NH_2

DOX conjugation was verified using ^{1}H NMR spectroscopy (23). The yield of DOX-conjugated polymer synthesis was 78.9%, with a conjugation efficiency of 36.04%, as reported in our previous study (23).

Critical Micelle Concentration (CMC) of DOX Conjugated mPEG-b-PCL-CO-NH-NH_2

Critical micelle concentration (CMC) is a key parameter for assessing the stability of micellar formulations. Pyrene was used as a fluorescent probe to determine the CMC. Upon micelle formation, the excitation wavelength of pyrene shifts from 333 nm to 338 nm and the fluorescence intensity ratio at 338 nm and 333 nm (I_{338}/I_{333}) was plotted against the logarithm of polymer concentration (24). In our previous study, the CMC values of mPEG-b-PCL, and mPEG-b-PCL-CO-NH-NH_2 copolymers were found as 14.1×10^{-3} mg/mL, and 9.8×10^{-3} mg/mL, respectively (30). The CMC of DOX-conjugated mPEG-b-PCL-CO-NH-NH_2 copolymers was found as 7.1×10^{-3} mg/mL (Figure 1A). These results indicate that increased hydrophobicity in the copolymer decreases the CMC value, thereby enhancing the stability of micellar formulations.

Characterization of DOX Conjugated Micelles (DOX_{conj}-M) and DOX Loaded Micelles (DOX_{ld}-M)

DOX_{conj}-M were obtained from covalently DOX-conjugated copolymers, while DOX_{ld}-M were prepared from copolymers using the co-solvent evaporation method without sonication. All micelles were characterized by hydrodynamic diameter and zeta potential measurements. Figure 1B shows the size distribution of micelles. The hydrodynamic mean diameter of DOX_{conj}-M (Figure 1B) was 121.6±16.3 nm (n=3) with a polydispersity index (PDI) of 0.206, and the zeta potential was -6.61±1.49 (n=3). In contrast, DOX_{ld}-M had a hydrodynamic diameter of 265.3±25.6 nm (n=3) (Figure 1C), a PDI of 0.353, and a zeta potential of -10.75±0.78 (n=3). TEM micrographs (Figure 1D and 1E) confirmed that the micelles were uniform and spherical in shape. Compared to DOXconj-M, DOXld-M exhibited a larger hydrodynamic diameter, higher PDI, and more negative zeta potential.

The drug loading capacities of the micelles were found as 13.54% (±1.13) for DOX_{conj}-M (n=3), and 8.62% (±0.47) DOX_{ld}-M (n=3). Meanwhile, the encapsulation efficiency (EE) of DOX in DOX_{ld}-M was calculated as 83.32% (±4.54). The lower drug loading capacity of DOX_{ld}-M may be attributed to the micelle preparation technique, which affects stability and consequently the drug loading capacity of the micelles (31). For example, the use of water or polyvinyl alcohol (PVA) in the aqueous phase during preparation influences micelle stability. In most cases, the addition of PVA, which acts as a surfactant and reduces surface tension, enables the formation of more stable micelles compared to using pure water (31).

Moulahoum et al. (2022) reported DOX loading into micelles prepared from carboxylic acid-terminated mPEG-b-PCL copolymers. They achieved 38% EE with micelles having a hydrodynamic diameter of 145.6 nm (PDI = 0.386) and a zeta potential of -37.2 mV (32). In comparison, the micelle sizes obtained in our study differed: DOX_{conj}-M were smaller while DOX_{ld}-M were

larger than those reported. Furthermore, the zeta potentials of both micelles (DOX_{conj}-M, and DOX_{ld}-M) in our study were lower than the literature values, likely due to differences in the copolymers used. Specifically, Moulahoum et al. (2022) synthesized a copolymer with a molecular weight of 2510 Da (32), whereas the copolymer in our study had a molecular weight of 16 kDa. On the other hand, the EE of DOX_{ld}-M in our study was higher than previously reported.

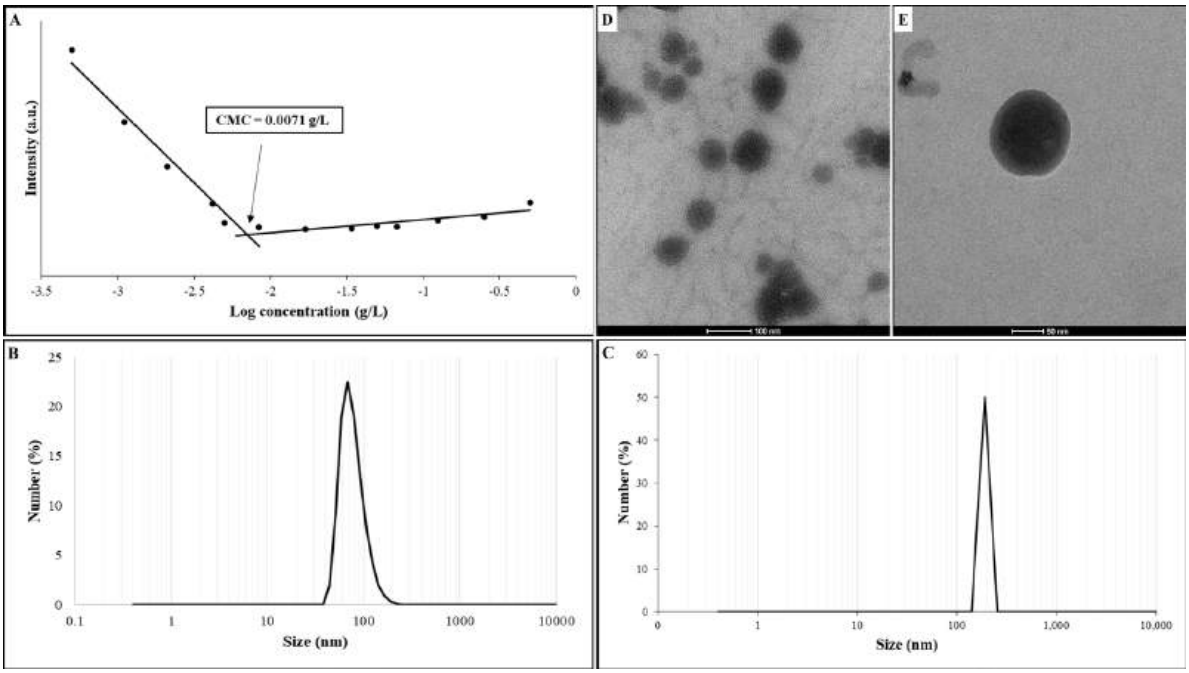

Figure 1. A) Plot of intensity ratio (I_{338}/I_{333}) of the excitation spectra of pyrene against log concentration of DOX conjugated copolymers (DOX_{conj}-M). The CMC of DOX-conjugated mPEG-b-PCL-CO-NH-NH_2 copolymers was found as 7.1×10^{-3} mg/mL. Size distribution charts of B) DOX_{conj}-M (121.6±16.3 nm, n=3) and C) DOX_{ld}-M (265.3±25.6 nm, n=3) prepared with 1% PVA – acetone. TEM images of D) DOX_{conj}-M, and E) DOX_{ld}-M prepared by co-solvent evaporation method without sonication using 1% PVA as water phase.

Release of DOX from DOX_{conj}-M or DOX_{ld}-M

In acidic media, the DOX release rate was higher for both DOX_{conj}-M and DOX_{ld}-M compared to neutral media (Figure 2).

For DOX_{conj}-M, no significant difference was observed between the release profiles at pH 7.4 and pH 6.8 in the first 2 days (Figure 2A). However, after this period, a significant increase in the release rate was observed at pH 6.8 ($p<0.05$). Moreover, DOX release was significantly faster at pH 5.0 than at the other tested conditions after 2 h ($p<0.05$). This shows that pH sensitive hydrazone bonds break in acidic environments, thereby increasing the amount of DOX released.

For DOX_{ld}-M, no significant difference was observed between the release profiles up to 2 h. Afterward, the DOX release rate significantly increased at pH 5.0 and pH 6.8 compared to physiological pH ($p<0.05$) (Figure 2B). Moreover, after 5 h, the release was significantly higher at pH 5.0 compared to pH 6.8 ($p<0.05$). This may be attributed to the increased solubility of DOX in acidic media.

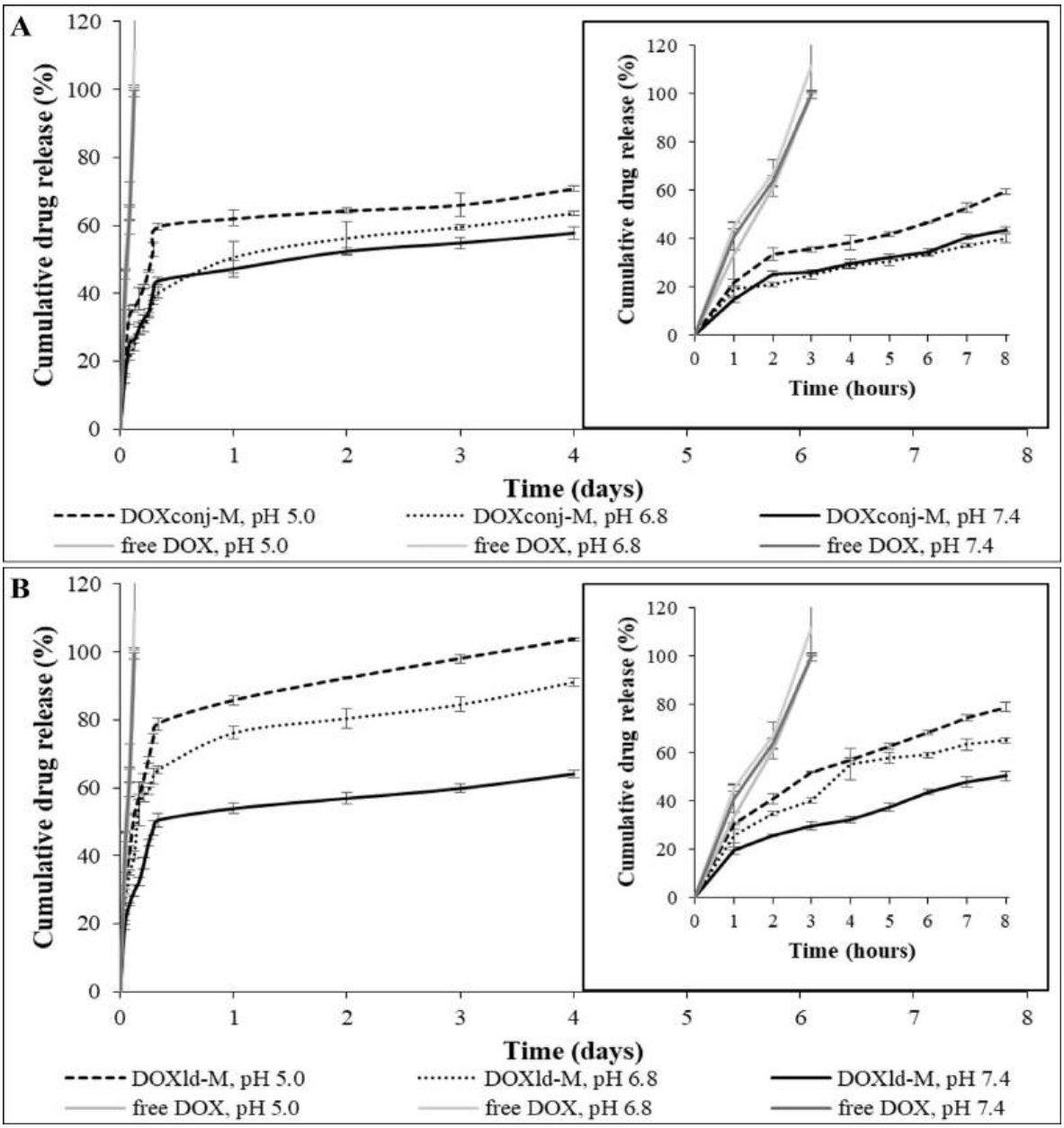

Figure 2. Cumulative drug release profiles from dialysis membrane of A) free DOX and DOX_{conj}-M; B) free DOX and DOX_{ld}-M under physiological conditions (PBS, 0.1 M and pH 7.4) and acidic conditions (CPB-pH 5.0 and CPB-pH 6.8; 0.15 M) at 37°C (n=6).

The release of free DOX through a dialysis membrane was also examined, showing much faster release compared to micelle formulations. Similar results showing fast release in acidic conditions were reported in the literature. For example, Liao et al. (2021) conjugated DOX to poly(2-(diethylamino) ethyl methacrylate)-polypropargyl methacrylate via hydrazone bonds and prepared micelles from the conjugated polymer. In acidic environments, the diethylamino groups of poly(2-(diethylamino) ethyl

methacrylate) become protonated, facilitating faster DOX release, while hydrazone bonds are also cleaved under acidic conditions. Thus, they achieved a dual pH responsive system combining hydrazone-bonded DOX and charge-reversible polymers. They reported DOX release rates of 63.43% at pH 5.0, 28.48% at pH 6.8, and 13.18% at pH 7.4 after 48 h (33).

In our study, higher burst release was observed in DOX_{ld}-M compared to DOX_{conj}-M. Within the first 8 h at pH 5.0, DOX release values were 60% for DOX_{conj}-M and 79% for DOX_{ld}-M. At pH 6.8, the release was 40% for DOX_{conj}-M and 61% for DOX_{ld}-M, while at pH 7.4, it was 41%, and 51%, respectively. The slower release of DOX_{conj}-M is likely due to the covalent attachment of DOX via hydrazone bonds, which reduces the release rate. After 48 h, 52% and 64% of DOX were released from DOX_{conj}-M at physiological pH and pH 5.0, respectively, compared to 57% and 92% from DOX_{ld}-M. At pH 5.0, complete DOX release (100%) occurred from DOX_{ld}-M within 4 days, whereas only ~70% release was achieved from DOX_{conj}-M (Figure 2).

Qi et al. (2018) prepared DOX-loaded pH-sensitive micelles with PEG-dihydrazone-PLA. They also prepared DOX-loaded PLA-PEG-PLA micelles to compare the effectiveness of dihydrazone bonds under acidic conditions. Their results showed that at pH 7.4, DOX release was 40% from PLA-PEG-PLA micelles and 38% from PEG-dihydrazone-PLA micelles, while at pH 5.0 the values were 40% and 75%, respectively. The reported results showed a pH sensitive drug delivery system with dihydrazone bonds (34).

Table 3. *In vitro* release kinetic parameters of DOX_{conj}-M and DOX_{ld}-M.

Micelles	Release Kinetic Models		pH 7.4	pH 6.8	pH 5.0
DOX_{conj}-M	Zero order	K_0	0.617	0.683	0.557
		R^2	-1.387	-1.741	-3.210
	First order	K_1	-0.009	-0.008	-0.006
		R^2	0.616	0.679	0.933
	Higuchi model	K_H	7.8552	0.111	9.885
		R^2	0.240	0.778	-0.028
	Korsmeyer-Peppas model	K_P	0.163	0.198	0.199
		n (exponent of release)	0.232	0.203	0.130
		R^2	0.926	0.951	0.478
DOX_{ld}-M	Zero order	K_0	0.739	1.012	1.140
		R^2	-1.669	-1.577	-0.794
	First order	K_1	-0.008	-0.008	-0.10
		R^2	0.612	0.598	0.919
	Higuchi model	K_H	8.791	0.069	14.225
		R^2	0.097	0.647	0.095
	Korsmeyer-Peppas model	K_P	0.208	0.278	0.254
		n (exponent of release)	0.215	0.222	0.238
		R^2	0.920	0.913	0.518

Our findings similarly showed that DOX release was faster under acidic conditions, and DOX conjugation (DOX_{conj}-M) resulted in slower drug release compared to DOX loading (DOX_{ld}-M). These results confirm the pH-responsive nature of DOXconj-M due to hydrazone bonds, which cleave in acidic environments, as expected. DOXld-M also showed pH-sensitive behavior, likely due to the higher solubility of DOX under acidic conditions compared to physiological conditions.

The release data were fitted to various kinetic models to determine the most suitable model for describing the release profile of DOX from the micelles. The rate constants (K0, K1, KH, and KP for zero-order, first-order, Higuchi, and Korsmeyer-Peppas models, respectively), the release exponent (n) values, and coefficient of determination (R2) were presented in Table 3. The Korsmeyer-Peppas model, which shows that drug release occurs from a polymeric system, provided the best fit for the release profiles of both micelles at pH 7.4 (PBS, 0.1 M and pH 7.4) and pH 6.8 (CPB, 0.15 M and pH 6.8). In contrast, the first-order model, which reflects a faster release behavior, was the best fit for the release of DOX from both micelles under acidic conditions (CPB, 0.15 M and pH 5.0).

In Vitro Cell Culture Experiments

Determination of IC_{50} of DOX on MDA-MB-231 Cells

Figure 3A presents the cell viability results of MDA-MB-231 cells. The IC50 value of DOX was calculated using GraphPad Prism 8 software and was determined to be 79.98 ± 4.37 nM. In the literature, IC50 value

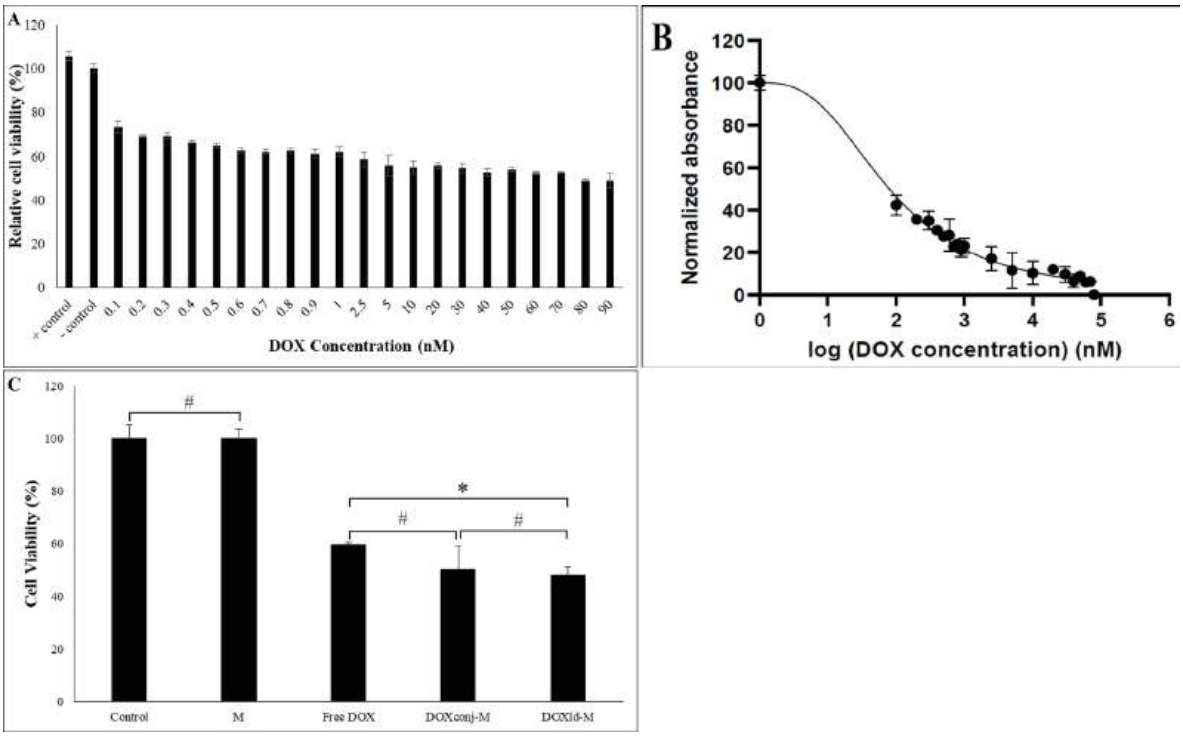

Figure 3. A) Cell viability results of MDA-MB-231 cells after treatment with different concentrations of DOX (n=4). B) Normalized absorbance vs. DOX concentration charts of MDA-MB-231 cells after data fitting using GraphPad Prism 8 software. C) Cytotoxic effect of DOX_{conj}-M and DOX_{ld}-M compared to free DOX (80 nM) on MDA-MB-231 cells (n=4). * shows the significant difference between the groups and # shows the non-significant difference between the groups ($p<0.05$; n=4)

of DOX on MDA-MD-231 cells has been reported as 1262 nM (35). The lower IC50 value observed in our study may be attributed to differences cell passage numbers or variations in cell line characteristics during culture. Figure 3B shows the normalized absorbance versus DOX concentration curves for MDA-MB-231 cells. The coefficient of determination (R^2) was 0.9575, indicating that the data closely fit the regression line (Figure 3B).

Cytotoxicity of DOX_{conj}-M and DOX_{ld}-M on MDA-MB-231 Cells

The viability of MDA-MB-231 cells was assessed after treatment with DOX_{conj}-M and DOX_{ld}-M to examine the effects of different drug loading mechanisms in the micelles (Figure 3C). The results showed that both DOX_{conj}-M and DOX_{ld}-M reduced cell viability, with no significant difference between the two groups. Although 1.5 mg/mL of DOX_{conj}-M and DOX_{ld}-M contained 374 µM and 238 µM of DOX, respectively, this did not result in a difference in cell viability. This outcome is consistent with the IC_{50} study of free DOX, where increasing the DOX concentration above the IC_{50} (80 nM) did not further reduce cell viability.

Cancer cells possess several mechanisms of drug resistance, including drug efflux. Due to the high mutation rate in cancer cells, multidrug resistance transporter proteins may actively expel drugs from the cell to prevent cytotoxicity (36,37). When DOX enters the cell via endocytosis, it can be recognized and removed by efflux mechanisms. Although the MDA-MB-231 cells used in this study are not classified as DOX resistant, prolonged passage numbers such as 25–30 may have contributed to acquired resistance. Ciocan-Cartita et al. (2020) studied the effect of passage number on mutagenicity of MDA-MB-231 cells and showed that mutations increased in passages 12 and 24 compared to passage 0. They also showed that increasing number of passages increased expression of drug resistance genes (38).

In our study, DOX_{ld}-M caused a significant decrease in cell viability compared to free DOX. However, DOX conjugation or loading had similar effects on MDA-MB-231 cells. DOX_{conj}-M had a higher drug loading capacity but a slower release rate than DOX_{ld}-M, which may explain the comparable cell viability observed for these groups.

Determination of Cell Internalization of Micelles

Cell internalization of free DOX began after 1 h and reached maximum levels at 4 h (Figure 4A). Similarly, DOX_{conj}-M was internalized after 1 h and reached peak internalization at 4 h (Figure 4B). Figure 4C shows the internalization of DOX_{ld}-M, which localized in the cell nuclei within 1 h. Overlap of DOX fluorescence with DAPI (dye for cell nuclei) staining in the images resulted in a purple coloration of the nuclei.

DOX_{ld}-M showed a different internalization pattern compared to DOX_{conj}-M and free DOX. As shown in the release studies, DOX release from DOX_{ld}-M was faster than from DOX_{conj}-M suggesting that after internalization, DOX_{ld}-M can deliver more DOX into the nuclei. Similar observations were reported by Cai et al. (2014) using DOX-conjugated hyaluronan nanoparticles (39) and Okur et al. (2016) with DOX-loaded PEG-dextran nanoparticles (40). These studies both reported cell nucle localization of DOX loaded nanoparticles. It is also known that DOX cause DNA damage in cells (41,42), so cell nuclei internalization of DOX_{ld}-M shows that these micelles may have high therapeutic potential in breast cancer treatment.

Cell Migration Assay

To simulate cancer cell migration in vitro, a transwell migration assay was carried out (Figure 4D and 4E). The results showed that the cell number at the bottom of the transwell decreased after treatment with free DOX, DOX_{conj}-M, and DOX_{ld}-M. While the cell numbers were similar for DOX_{conj}-M and DOX_{ld}-M treatments, both groups exhibited a significantly greater inhibition of migration compared to free DOX.

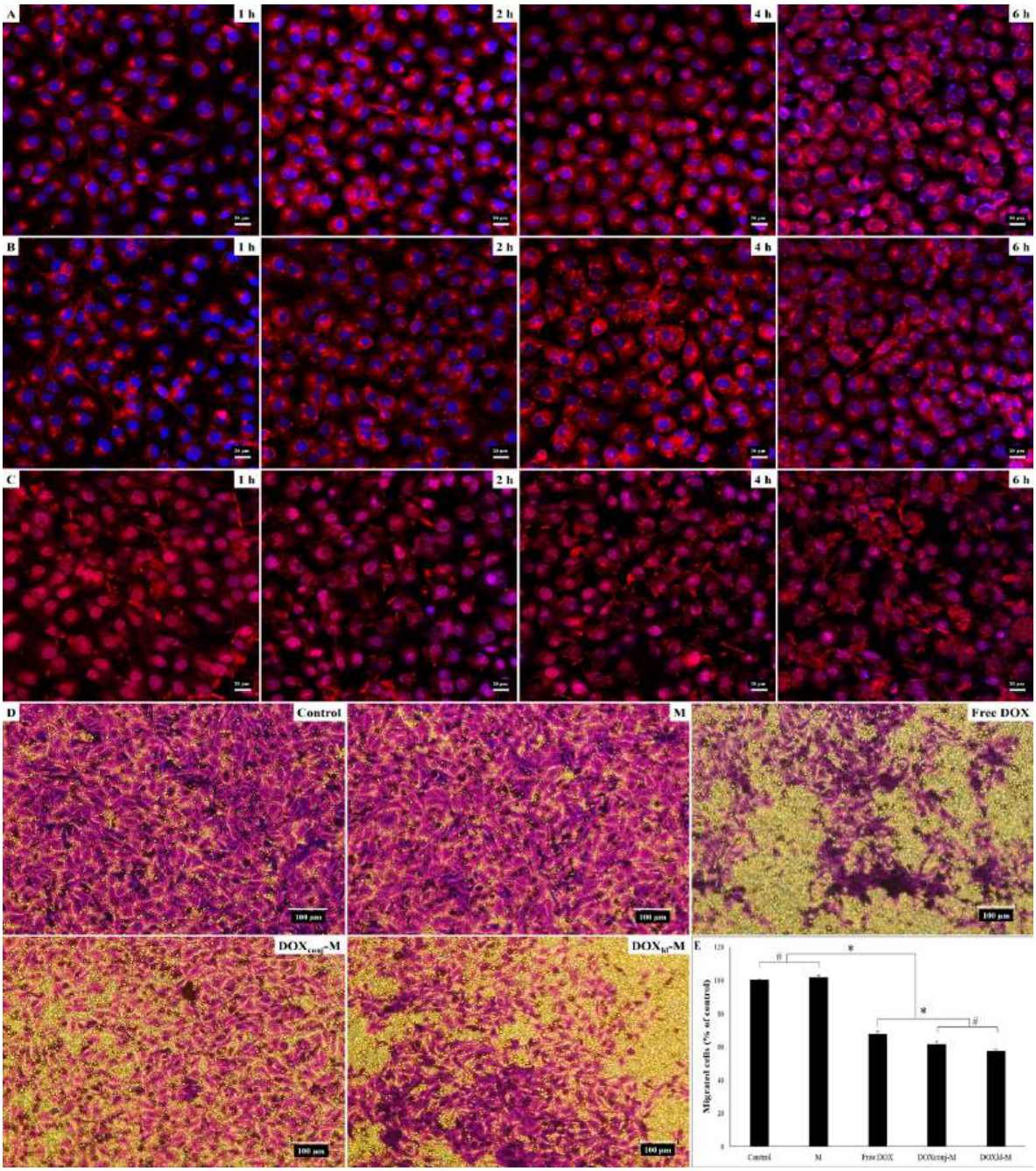

Figure 4. Cell internalization after 1h, 2h, 4h and 6h of A) free DOX, B) DOX_{conj}-M, and C) DOX_{td}-M. Cell nuclei was stained with DAPI. Blue is DAPI, and red is DOX in images. D) Images of MDA-MB-231 cells migrated from the top of the transwell to the bottom of the transwell after treatment. E) Normalized plot of migrated cells after transwell migration assay. IC_{50} concentration of DOX (80 nM) was used in free DOX group. Transwell migration assay was carried out for 48 hours and then, cells were fixed with 4% paraformaldehyde and stained with 0.2% crystal violet. After that, cells were counted from three independent experiments. * shows the significant difference between the groups and # shows the non-significant difference between the groups ($p<0.05$; n=3).

Colony Formation Assay

To evaluate the anti-proliferative effects of micelles (DOX_{conj}-M, and DOX_{ld}-M), a colony formation assay was carried out (Figure 5A). The results showed that both micelle formulations showed similar anti-proliferative effects to free DOX, while the control (untreated) and M (empty micelles) groups displayed the highest proliferation. Xie et al. (2019) co-loaded DOX and miR-34a into micelles prepared from polyethylenimine-polycaprolactone and gadolinium(III)-conjugated polyethyleneglycol-polycaprolactone. In their study, colony formation assays on MDA-MB-231 cells showed that micelles containing 15 μM DOX reduced colony numbers by approximately 30%, whereas micelles containing both 15 μM DOX and miR-34a reduced colony numbers by approximately 55% (43).

In our study, DOX_{conj}-M and DOX_{ld}-M contained 374 μM and 238 μM DOX, respectively, which are considerably higher amounts of DOX compared to the micelles prepared by Xie et al. (2019). Consistently, both DOX_{conj}-M and DOX_{ld}-M decreased the colony-forming ability of MDA-MB-231 cells by 50%. This enhanced inhibition may be attributed to the higher DOX content of our micelles, despite the absence of miR-34a co-loading.

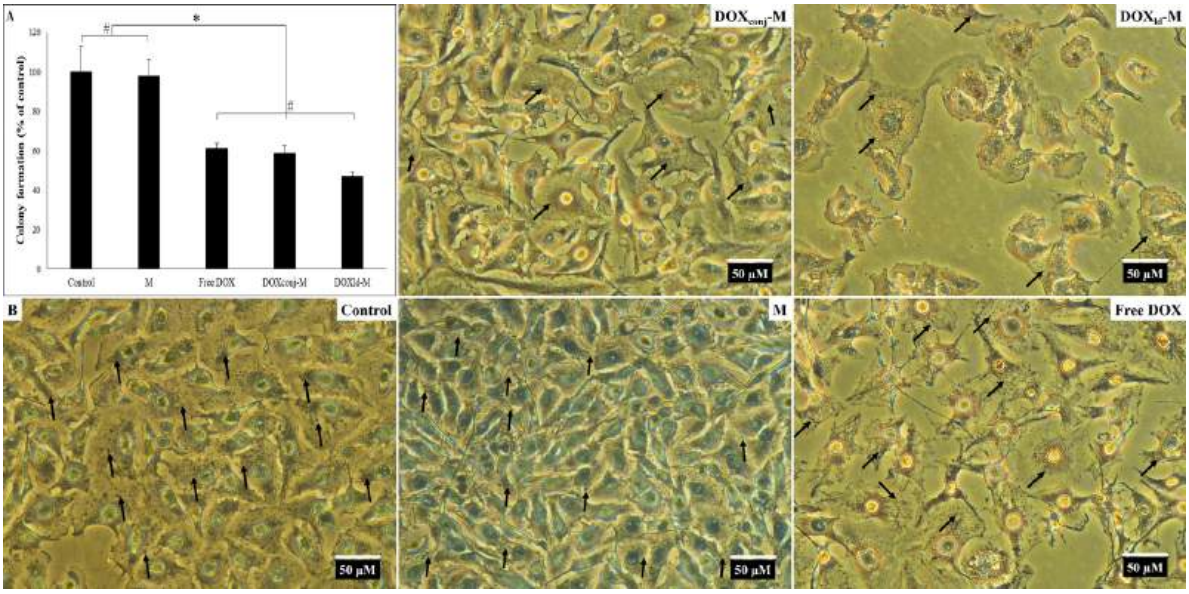

Figure 5. A) Normalized plot of colonies after colony formation assay. IC_{50} concentration of DOX (80 nM) was used in free DOX group. Colony formation assay was carried out for a week and then, colonies were counted manually from three independent experiments. * shows the significant difference between the groups and # shows the non-significant difference between the groups ($p<0.05$; n=3). B) Images of MDA-MB-231 cells stained for lipid droplets with oil red after treatment. Hematoxylin was used to counterstain the cells. IC_{50} concentration DOX (80 nM) was used in free DOX group. Black arrows show the lipid droplets. They are seen as small gray dots inside the cells (in the cytoplasm).

Determination of Lipid Droplets in MDA-MB-231 Cells

Lipid droplet formation shows the proliferation ability of breast cancer cells. To assess the lipid droplet formation in MDA-MB-231 cells, the cells were stained with oil red O and hematoxylin after incubation with free DOX, M, DOX_{conj}-M, and DOX_{ld}-M for 48 h (Figure 5B). The results showed that none of the treatments altered lipid droplet formation, although changes in cell morphology were observed.

Cells in the DOX-treated groups appeared enlarged compared to the control and M groups. Similar findings have been reported in the literature: Mehdizadeh et al. (2017) treated hepatocellular carcinoma and colorectal cancer cells with DOX and after oil red O staining, observed that treatment with DOX did not decrease lipid droplet formation, but, on the contrary, increased it (44).

Detection of Apoptosis in Cancer Cells with qRT-PCR

During apoptosis, the expression of pro-apoptotic genes such as Bax and p53 increases, while the expression of anti-apoptotic genes Bcl-2 and Bcl-xL decreases. Therefore, we investigated the apoptotic effect of free DOX, DOX_{conj}-M, and DOX_{ld}-M on MDA-MB-231 cells (Figure 6A, 6B, 6C, and 6D). Free DOX demonstrated higher Bax gene expression compared to all other groups (Figure 6A). However, there was no significant difference in Bax expression between DOX_{conj}-M and DOX_{ld}-M (Figure 6A). In all groups, Bax expression was higher compared to the control (untreated cells) and M groups (Figure 6A). Free DOX also yielded the highest p53 expression (Figure 6B). Both DOX_{conj}-M and DOX_{ld}-M increased p53 expression compared to the control and M groups, with DOX_{conj}-M inducing greater expression than DOX_{ld}-M (Figure 6B). Free DOX and DOX_{conj}-M both elevated Bcl-2 (Figure 6C) and Bcl-xL (Figure D) expressions, whereas DOXld-M significantly reduced their expression. Abdel-Hakeem et al. (2020) similarly reported that DOX-loaded chitosan-protamine nanoparticles reduced Bcl-2 expression in MDA-MB-231 cells more effectively than free DOX (45). In our study, cell internalization results showed that DOXld-M localized in the cell nuclei, potentially causing greater DNA damage due to DOX release within the nucleus compared to DOX_{conj}-M. Lower Bcl-2 and Bcl-xL expressions observed with DOX_{ld}-M may therefore result from this higher DNA damage. Although both micelle types promoted apoptosis, DOXld-M was found to be more effective than DOX_{conj}- M.

Determination of Cell Apoptosis with Annexin V-FITC Assay

Apoptosis of MDA-MB-231 cells after treatment with free DOX, DOX_{conj}-M, and DOX_{ld}-M was evaluated using the Annexin V-FITC assay (Figure 6E, and 6F). All three treatments significantly increased apoptosis compared to the control and M groups. The highest number of apoptotic cells was observed in the DOX_{ld}-M group, while no significant difference was detected between free DOX and DOX_{conj}-M. In line with our findings, Gao et al. (2017) prepared DOX- and honokiol-containing mPEG-b-PCL micelles and evaluated their effects on apoptosis. Honokiol, known for its antioxidative, anti-inflammatory, and potential anticancer properties, did not induce apoptosis in C6 glioma cells when delivered in micelles. In contrast, DOX-loaded and DOX-honokiol co-loaded micelles significantly increased apoptosis (46). In our study, all DOX-containing formulations induced apoptosis, which is consistent with our qRT-PCR and ROS generation results.

3.6.9. Mitochondrial Transmembrane Potential Detection

DiOC6 was used as the fluorescent probe which binds to intact mitochondria, where a decrease in fluorescence intensity indicates loss of mitochondrial transmembrane potential, ultimately leading to apoptosis. In Figure 6G, mitochondrial transmembrane potential analysis results are given. Treatment with free DOX, DOXconj-M, and DOXld-M decreased mitochondrial transmembrane potential by 44.4 ± 0.7%, 41.8 ± 2.8%, and 43.0 ± 1.7%, respectively. These findings indicated that all DOX-containing micelles caused mitochondrial dysfunction, which can trigger apoptosis through the release of apoptotic proteins. Similarly, Zeng et al. (2014) demonstrated that DOX-loaded nanoparticles prepared from Boltorn® H30-based hyperbranched dendritic-linear copolymers reduced mitochondrial transmembrane potential in MCF-7 cells (47).

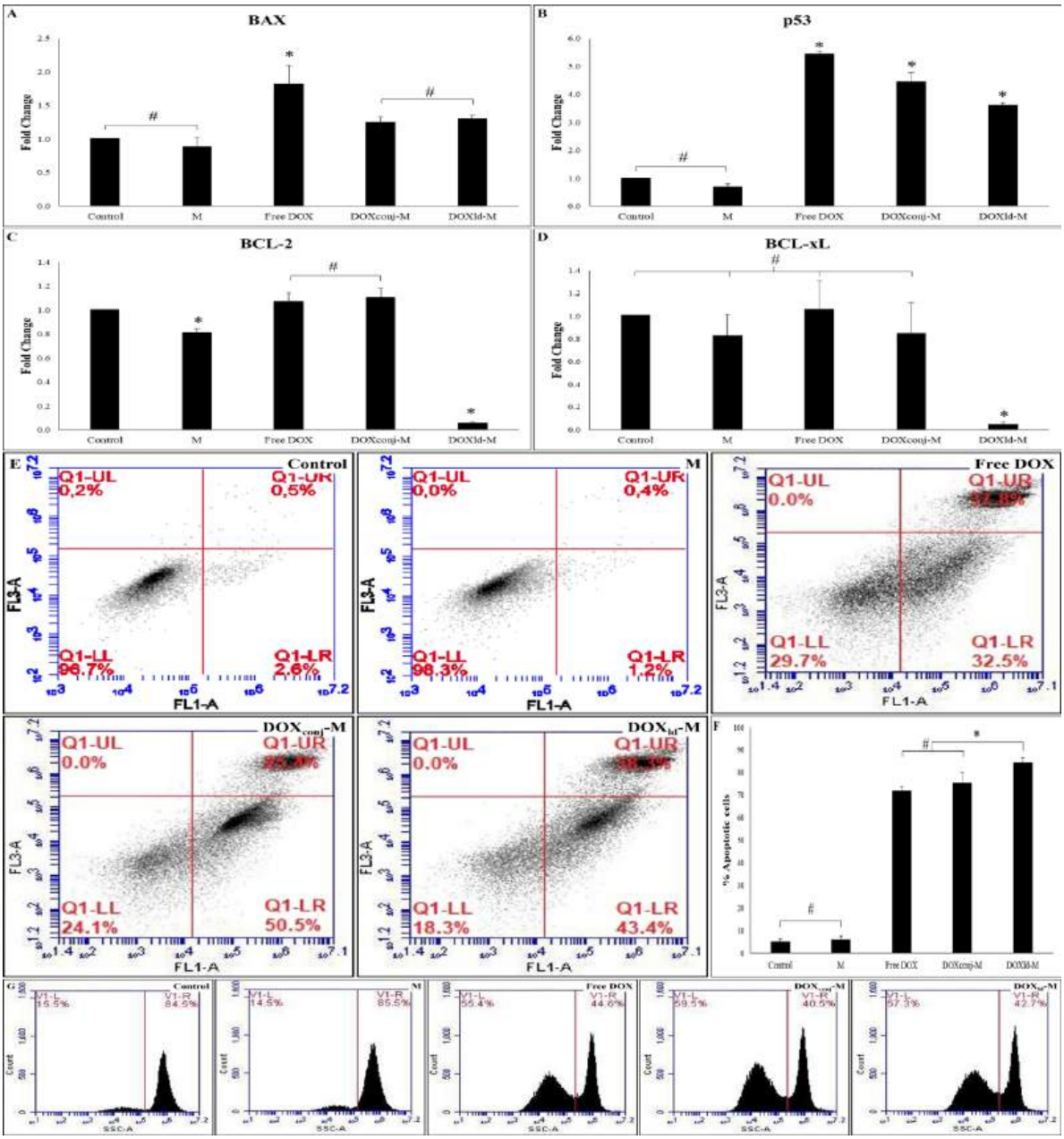

Figure 6. qRT-PCR results of A) Bax, B) p53, C) Bcl-2, and D) Bcl-xL genes of MDA-MB-231 cells after free DOX, DOX_{conj}-M, DOX_{ld}-M, and M treatment for 24 hours (n=3). IC_{50} concentration of DOX (80 nM) was used in free DOX group. * shows the significant differences between the groups ($p<0.05$) and # shows non-significant differences ($p>0.05$). E) Annexin-V/FITC apoptosis assay results of MDA-MB 231 cells without treatment (control group: untreated cells), after treatment with M, free DOX, DOXconj-M, and DOXld-M for 24 h. Q1-LL: viable cells. Q1-UL: dead cells. Q1-UR: late apoptotic cells. Q1-LR: early apoptotic cells. F) Percentage of apoptotic cells after 24 h incubation (n=3). IC_{50} concentration of DOX (80 nM) was used in free DOX group. * shows the significant differences ($p<0.05$) between the groups and # shows the nonsignificant differences ($p>0.05$). G) Mitochondrial transmembrane potential measurements of MDA-MB-231 cells without treatment (control group: untreated cells) using DiOC6, after treatment with M, free DOX, DOX_{conj}-M, and DOX_{ld}-M for 24 h using DiOC6.

Reactive Oxygen Species (ROS) Determination

DCFDA, a fluorescent probe, was used to detect intracellular ROS. In this study, ROS fluorescence was determined with confocal microscopy, and the results showed that free DOX, DOX_{conj}-M, DOX_{ld}-M, and TBHP all increased ROS levels compared to the control and M groups (Figure 7A). TBHP served as a positive control since it generates radical species that elevate ROS levels in cells. ROS levels were further quantified by measuring fluorescence intensity (Figure 7B). Among the groups, DOX_{conj}-M induced the highest ROS generation. DOX_{ld}-M significantly increased ROS generation compared to free DOX group. These results showed that DOX-conjugated and DOX-loaded micelles enhanced ROS generation more effectively than free DOX, potentially contributing to stronger apoptotic activity, as ROS generation is an early hallmark of apoptosis. Cheng et al. (2020) prepared DOX-loaded mixed micelles from Pluronic F127 and phenylboronic ester-grafted Pluronic P123.

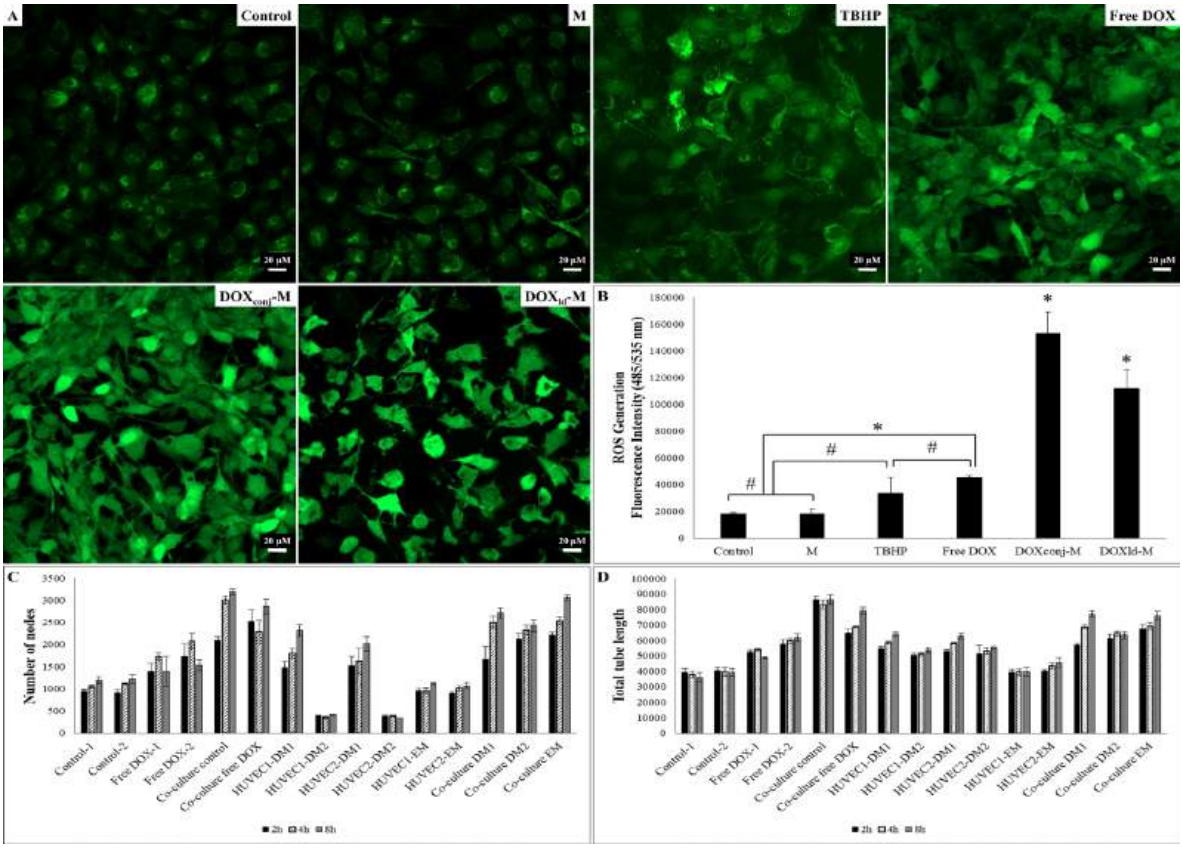

Figure 7. CA) ROS determination with confocal microscopy after treatment with TBHP, M, free DOX, DOX_{conj}-M, and DOXld-M for 24 h (TBHP: Tert-butyl hydroperoxide). B) ROS determination by measuring fluorescence intensity using microplate reader after treatment with TBHP, M, free DOX, DOX_{conj}-M, and DOX_{ld}-M for 24 h (n=4). * shows the significant differences between the groups ($p<0.05$) and # shows non-significant differences ($p>0.05$). DCFDA is a green fluorescent dye that stains ROS in cells. C) Quantification of tube formation in terms of number of nodes. D) Quantification of tube formation in terms of total tube lengths. IC_{50} concentration (80 nM) was used in free DOX group. Images of HUVECs were taken after 2, 4, and 8 hours of incubation at 37°C from three independent experiments and number of nodes and total tube length were measured using ImageJ software (n=3). 1: EC medium, 2: EC:L15 medium (1:1), EM: mPEG-b-PCL micelles (M), DM1: DOX_{conj}-M, DM2: DOX_{ld}-M

Phenylboronic ester was used to give ROS sensitivity to micelles. They reported that ROS-insensitive and ROS-sensitive DOX-loaded mixed micelles increased ROS generation in DOX-resistant MCF7 cells by 5.49- and 8.96-fold, respectively, compared to free DOX (48). In our study, DOX_{conj}-M and DOX_{ld}-M increased ROS generation compared to free DOX by 3.37-fold and 2.47-fold, respectively. These results showed that DOX-containing micelles can increase the effectiveness of DOX in resistant cells. Furthermore, as shown in Figure 7A, DOX_{ld}-M decreased cell numbers more than DOX_{conj}-M, and morphological changes appeared more pronounced, suggesting that DOX_{ld}-M induced stronger ROS generation than DOX_{conj}-M.

Endothelial Cell Tube Formation Assay

Cancer cells overexpress vascular endothelial growth factors (VEGFs) to stimulate angiogenesis, thereby improving access to nutrients. Tube formation assay was carried out to determine the effects of DOX- containing micelles on angiogenesis. The results showed that co-culture of MDA-MB-231 cells with HUVECs significantly stimulated tube formation (Figure S1, Figure S2, Figure S3 and Figure S4). Free DOX further increased tube formation compared to control groups, whereas both DOXconj-M, and DOXld-M reduced tube formation relative to free DOX.

There were more meshes in co-cultures of MDA-MB-231 cells with HUVECs compared to the control groups (untreated cells) which means that cancer cells promoted the vessel formation of endothelial cells. Co-culture of endothelial cells with cancer cells increases angiogenesis of endothelial cells, because cancer cells overexpress some growth factors like VEGF. Breast cancer cells also overexpress VEGF, which results in new blood vessel formation and increased permeability of vessels, which causes metastasis. In brain, the vessels present in 'blood-brain barrier' decrease permeability. This prevents brain from components as well as bioactive agents and drugs in the circulating blood. Metastatic breast cancer cells increase the permeability of these vessels in the blood-brain barrier, thereby promoting brain metastasis.

Treatment with empty micelles (M) resulted in similar mesh formation as the control groups (untreated cells). Free DOX significantly increased the number of nodes and total tube length compared to both the control and co-culture control groups (Figure 7C, and 7D). Among the DOX-containing micelles, DOXconj-M caused in the highest number of nodes, whereas DOXld-M produced the lowest. Importantly, micelles containing DOX did not differ significantly from the control in terms of number of nodes and total tube length. In agreement with our findings, Shi et al. (2021) also showed that 500 nM of free DOX increased number of nodes compared to control cells (49).

No significant differences were observed in number of nodes between the co-culture control and co-cultures treated with empty micelles (M) after 2h and 8h of incubations. However, after 4h, co-culture control group had a significantly higher number of nodes than the co-culture group treated with empty micelles (M). Moreover, the total tube length of the co-culture control group was significantly higher than that of the groups treated with M at 2 h, 4 h, and 8 h.

DISCUSSION

In this study, a hydrazide-functionalized mPEG-b-PCL copolymer was synthesized, and micelles (M) were prepared using the solvent evaporation method without sonication. DOX was either physically loaded into these micelles or first covalently conjugated to the copolymer via pH-responsive hydrazone bonds before micelle formation, and then micelles were prepared. Characterization studies showed that all micelles exhibited a uniform shape with nanosized structures of approximately 100-200 nm, making them suitable for intravenous administration. Micelles were highly stable, as confirmed by zeta potential and polydispersity index analyses.

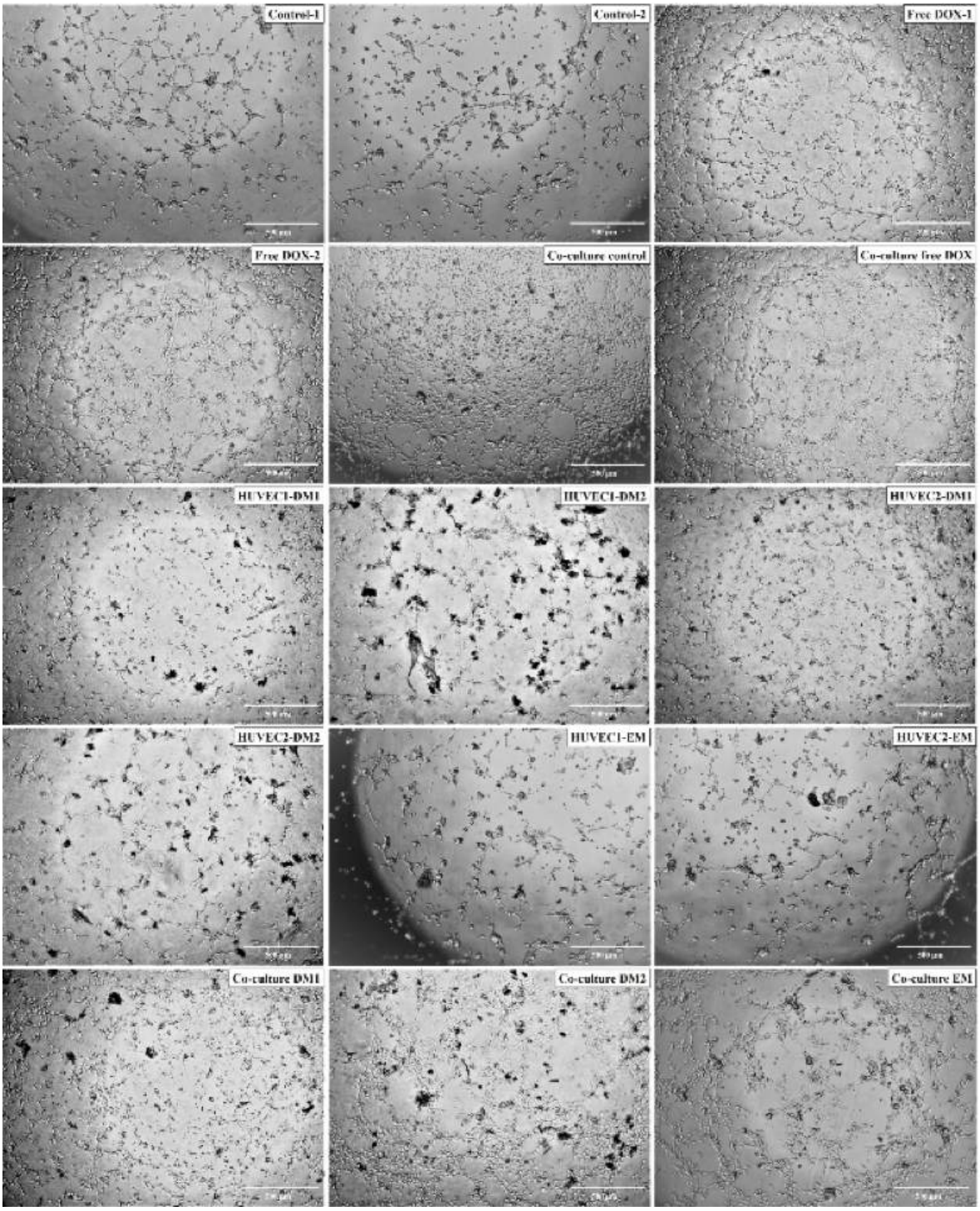

Figure S1. Images of tube formation assay after 2 hours of incubation. Scale bar is 500 µm. 40×10^3 HUVECs and 40×10^3 MDA-MB-231 cells were used in the experiments. 1: EC medium, 2: EC:L15 medium (1:1), EM: mPEG-b-PCL micelles (M), DM1: DOX_{conj}-M, DM2: DOX_{ld}-M

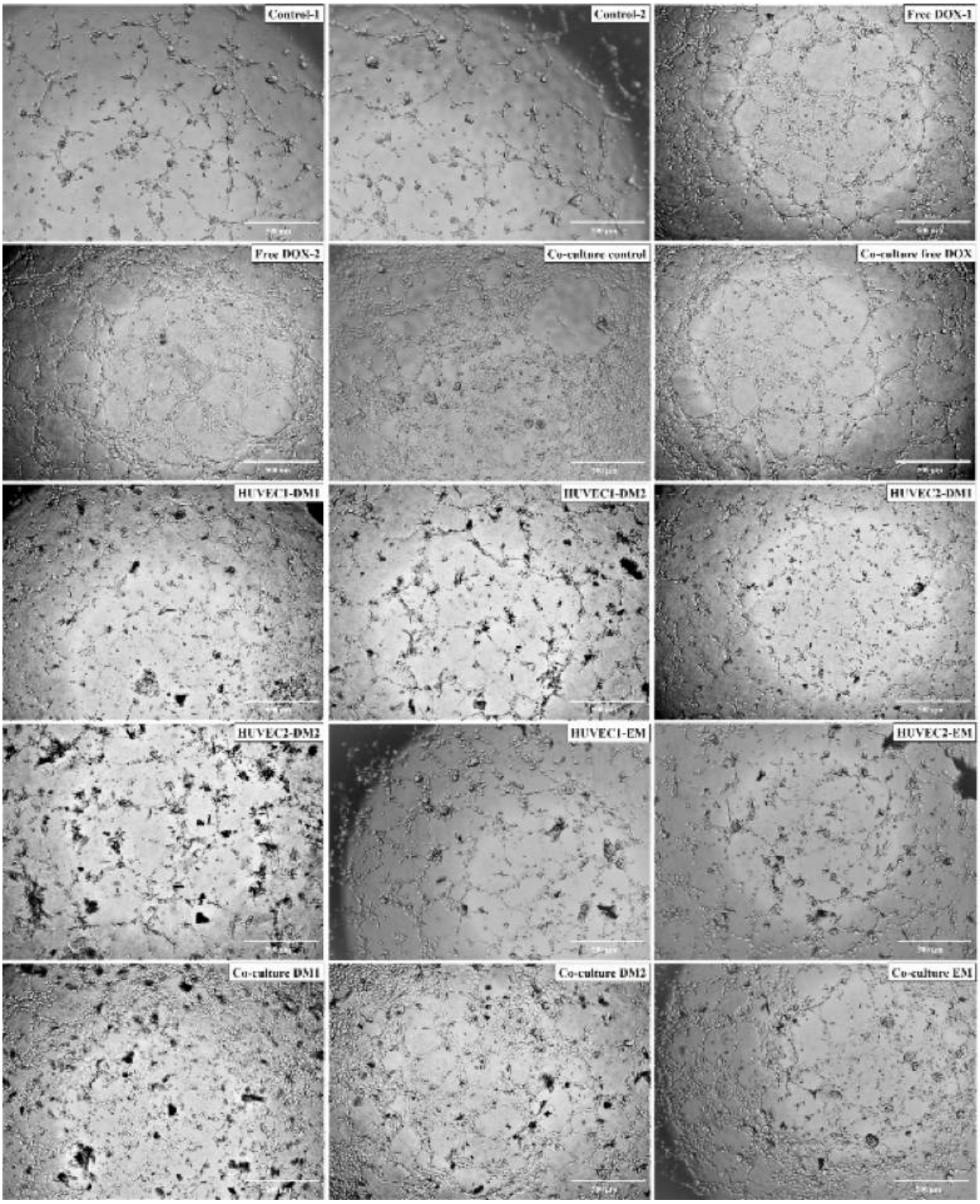

Figure S2. Images of tube formation assay after 4 hours of incubation. Scale bar is 500 µm. 40×10^3 HUVECs and 40×10^3 MDA-MB-231 cells were used in the experiments. 1: EC medium, 2: EC:L15 medium (1:1), EM: mPEG-b-PCL micelles (M), DM1: DOX_{conj}-M, DM2: DOX_{td}-M.

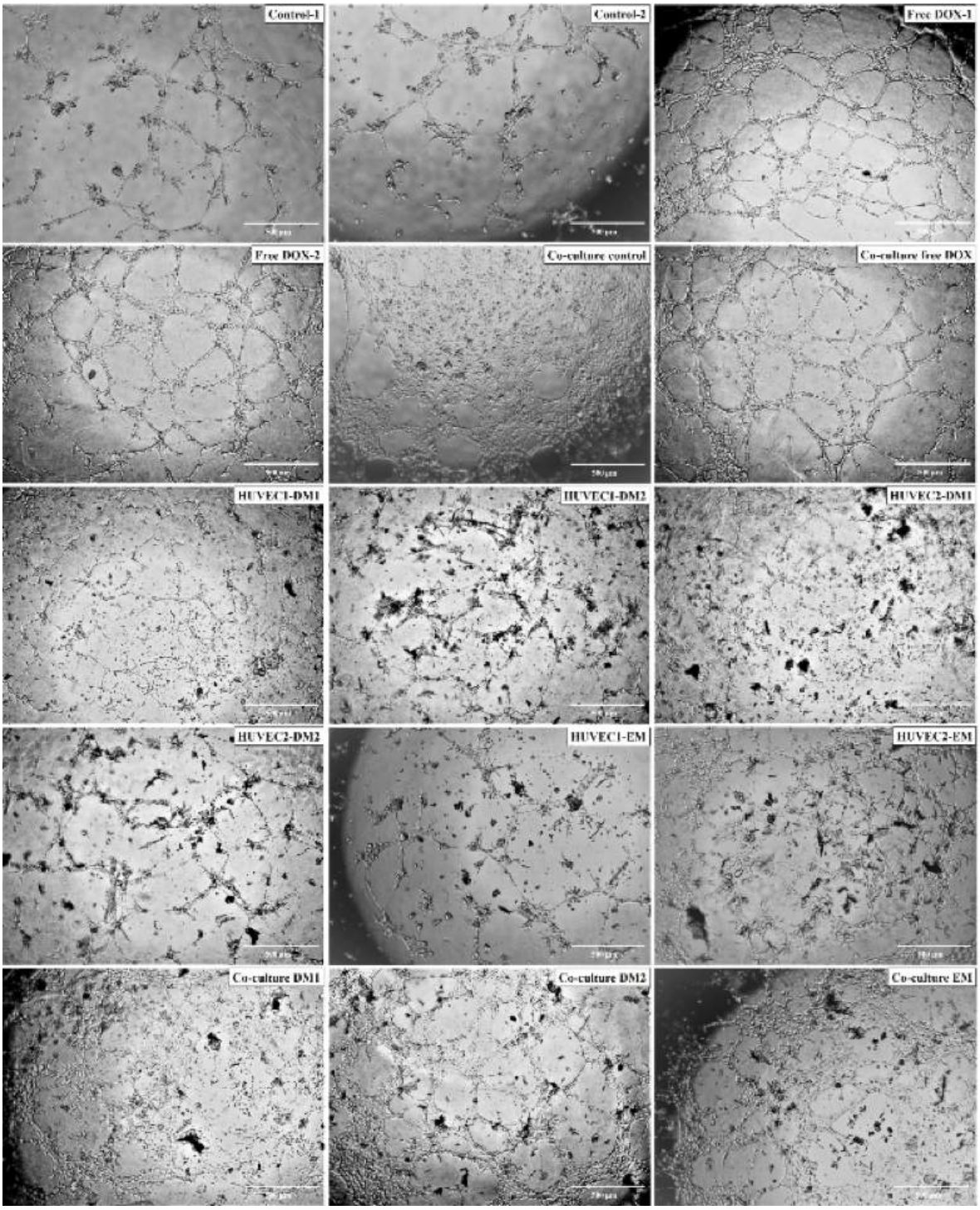

Figure S3. Images of tube formation assay after 8 hours of incubation. Scale bar is 500 µm. 40×10^3 HUVECs and 40×10^3 MDA-MB-231 cells were used in the experiments. 1: EC medium, 2: EC:L15 medium (1:1), EM: mPEG-b-PCL micelles (M), DM1: DOX_{conj}-M, DM2: DOX_{ld}-M.

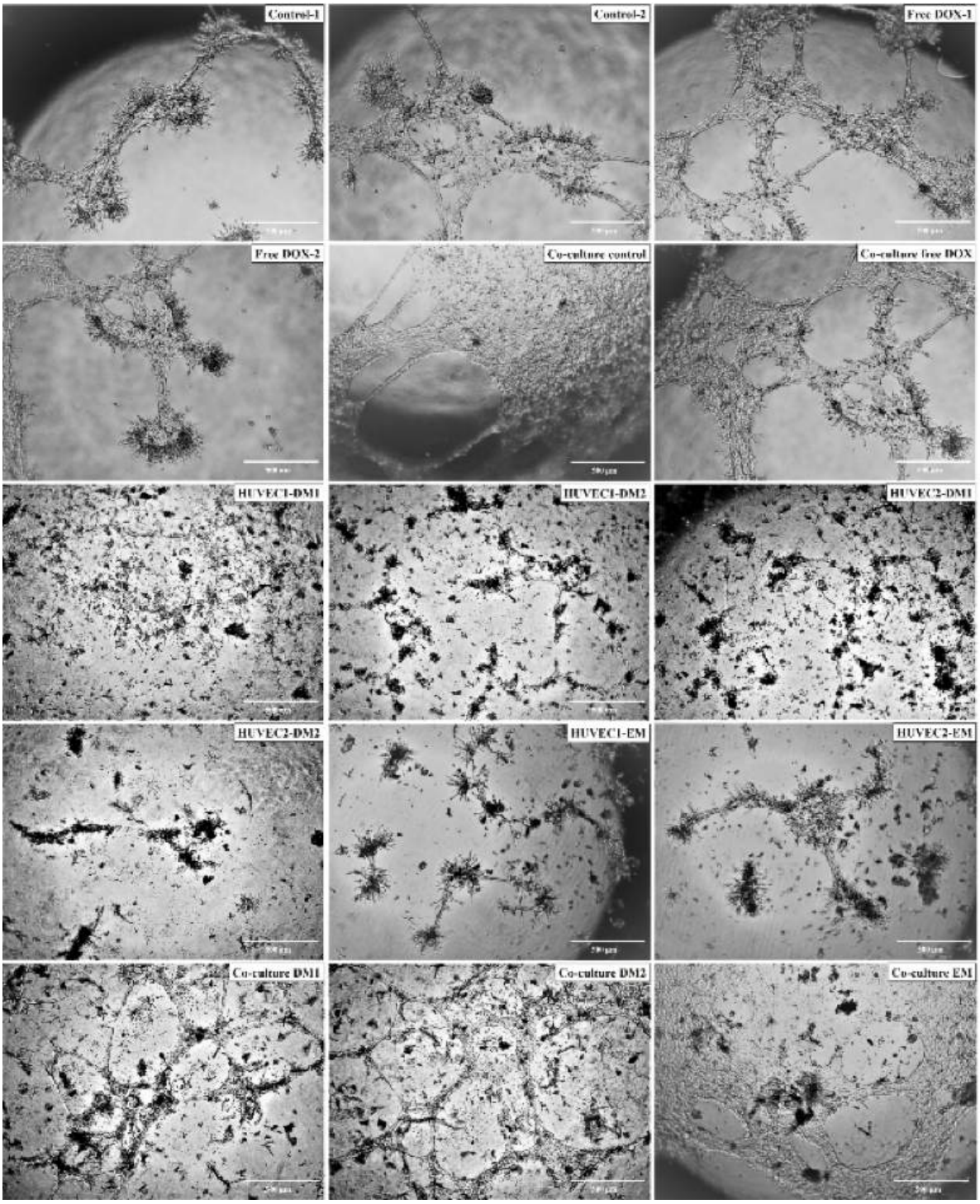

Figure S1. Images of tube formation assay after 24 hours of incubation. Scale bar is 500 µm. 40×10^3 HUVECs and 40×10^3 MDA-MB-231 cells were used in the experiments. 1: EC medium, 2: EC:L15 medium (1:1), EM: mPEG-b-PCL micelles (M), DM1: DOX_{conj}-M, DM2: DOX_{ld}-M.

Drug release studies showed pH-sensitive behavior, with DOX-conjugated micelles showing slower drug release compared to DOX-loaded micelles. All DOX-containing micelles demonstrated greater cytotoxic effects on MDA-MB-231 cells compared to the drug-free micelle control group. Furthermore, cell migration was reduced in all treatment groups. DOX_{ld}-M induced higher levels of apoptosis and reactive oxygen species (ROS) generation than DOX_{conj}-M. In addition, DOX-containing micelles caused a decrease in mitochondrial transmembrane potential, indicating apoptotic progression. Tube formation assays revealed that DOX_{ld}-M more effectively inhibited endothelial cell tube formation compared to DOX_{conj}-M.

In conclusion, pH-sensitive micelles were developed through both DOX conjugation via hydrazone linkage and DOX loading. Among these systems, DOX loading was found to be more effective against cancer cells than DOX conjugation. To show the effectiveness of these systems on cancer treatment, in vivo studies should be carried out.

ACKNOWLEDGEMENTS

The authors acknowledge BIOMATEN Center of Excellence in Biomaterials and Tissue Engineering and Central Laboratory of Middle East Technical University. The authors acknowledge TUBİTAK for Ph.D. scholarship.

FUNDING

This research was supported by METU BAP grant (Project No: GAP-310-2019-10184).

ETHICS COMMITTEE APPROVAL

* This study does not require Ethics Committee Approval.

CONFLICT OF INTEREST

The authors declare no conflict of interest.

REFERENCES

1. Kim HM, Lee J, Koo JS. Clinicopathological and prognostic significance of programmed death ligand-1 expression in breast cancer: A meta-analysis. BMC Cancer, 2017;17:690.

2. Parvani JG, Jackson MW. Silencing the roadblocks to effective triple negative breast cancer treatments by siRNA nanoparticles. Endocrine-Related Cancer, 2017;24(4):R81–97.

3. Chen W, Li L, Zhang X, Liang Y, Pu Z, Wang L, et al. Curcumin: a calixarene derivative micelle potentiates anti-breast cancer stem cells effects in xenografted, triple-negative breast cancer mouse models. Drug Deliv, 2017;24(1):1470–81.

4. Pelengaris S, Khan M. The Molecular Biology of Cancer: A Bridge From Bench to Bedside. 2nd ed. UK: John Wiley & Sons, Inc., 2013.

5. Li Y, Yang HY, Thambi T, Park JH, Lee DS. Charge-convertible polymers for improved tumor targeting and enhanced therapy. Biomaterials, 2019;217:119299.

6. Chang M, Zhang F, Wei T, Zuo T, Guan Y, Lin G, et al. Smart linkers in polymer-drug conjugates for tumor-targeted delivery. J Drug Target, 2016;24(6):475–91.

7. Faal Maleki M, Jafari A, Mirhadi E, Askarizadeh A, Golichenari B, Hadizadeh F, et al. Endogenous stimuli-responsive linkers in nanoliposomal systems for cancer drug targeting. Int J Pharm, 2019;572:118716.

8. Etrych T, Šubr V, Laga R, Říhová B, Ulbrich K. Polymer conjugates of doxorubicin bound through an amide and hydrazone bond: Impact of the carrier structure onto synergistic action in the treatment of solid tumours. European Journal of Pharmaceutical Sciences. 2014;58(1):1–12.

9. Lale S V., Kumar A, Naz F, Bharti AC, Koul V. Multifunctional ATRP based pH responsive polymeric nanoparticles for improved doxorubicin chemotherapy in breast cancer by proton sponge effect/endo-lysosomal escape. Poly Chem, 2015;6(11):2115-32.

10. Zhang YC, Zeng PY, Ma ZQ, Xu ZY, Wang ZK, Guo B, et al. A pH-responsive complex based on supramolecular organic framework for drug-resistant breast cancer therapy. Drug Deliv, 2022;29(1):1-9.

11. Wilczewska AZ, Niemirowicz K, Markiewicz KH, Car H. Nanoparticles as drug delivery systems. Pharm Rep, 2012;64(5):1020-37.

12. Wang Y, Wang Y, Chen G, Li Y, Xu W, Gong S. Quantum- dot-based theranostic micelles conjugated with an anti- EGFR nanobody for triple-negative breast cancer therapy. ACS Appl Mater Interfaces, 2017;9:30297-305.

13. Torchilin VP. Micellar nanocarriers: Pharmaceutical perspectives. Pharm Res, 2007;24(1):1-16.

14. Owen SC, Chan DPY, Shoichet MS. Polymeric micelle stability. Nano Today. 2012;7(1):53-65.

15. Senevirathne SA, Washington KE, Biewer MC, Stefan MC. PEG based anti-cancer drug conjugated prodrug micelles for the delivery of anti-cancer agents. J Mater Chem B, 2016;4(3):360-70.

16. Xiong W, Peng L, Chen H, Li Q. Surface modification of MPEG-b-PCL-based nanoparticles via oxidative self-polymerization of dopamine for malignant melanoma therapy. Int J Nanomed,. 2015;10:2985-96.

17. Mariani E, Lisignoli G, Borzì RM, Pulsatelli L. Biomaterials: Foreign bodies or tuners for the immune response? Int J Mol Sci, 2019;20:636.

18. Celentano W, Ordanini S, Bruni R, Marocco L, Medaglia P, Rossi A, et al. Complex poly(ε-caprolactone)/poly(ethylene glycol) copolymer architectures and their effects on nanoparticle self-assembly and drug nanoencapsulation. Euro Poly J, 2021;144:110226.

19. Zamani M, Rostamizadeh K, Kheiri Manjili H, Danafar H. In vitro and in vivo biocompatibility study of folate-lysine-PEG-PCL as nanocarrier for targeted breast cancer drug delivery. Euro Poly J, 2018;103:260-70.

20. Zhu W, Xie W, Tong X, Shen Z. Amphiphilic biodegradable poly(CL-b-PEG-b-CL) triblock copolymers prepared by novel rare earth complex: Synthesis and crystallization properties. Euro Poly J, 2007;43(8):3522-30.

21. El Jundi A, Buwalda S, Bethry A, Hunger S, Coudane J, Bakkour Y, et al. Double-Hydrophilic Block Copolymers Based on Functional Poly(ε-caprolactone)s for pH-Dependent Controlled Drug Delivery. Biomacromolecules, 2020;21(2):397-407.

22. Isik G, Hasirci N, Tezcaner A, Kiziltay A. Multifunctional periodontal membrane for treatment and regeneration purposes. J Bio Comp Poly, 2020;35(2):117-38.

23. Isik G, Tezcaner A, Hasirci N, Kiziltay A. Determination of doxorubicin amount conjugated to mPEG-b-PCL copolymer via pH sensitive hydrazone bond. Turkish Bull Hyg Expl Biol, 2022;In press.

24. Mohanty AK, Jana U, Manna PK, Mohanta GP. Synthesis and evaluation of MePEG-PCL diblock copolymers: surface properties and controlled release behavior. Progress in Biomaterials. 2015;4(2-4):89-100.

25. Aliabadi HM, Elhasi S, Mahmud A, Gulamhusein R, Mahdipoor P, Lavasanifar A. Encapsulation of hydrophobic drugs in polymeric micelles through co-solvent evaporation: The effect of solvent composition on micellar properties and drug loading. Int J Pharm, 2007;329(1-2):158-65.

26. He XL, Xing Y, Gu XZ, Xiao JX, Wang YY, Yi Z, et al. The synthesis and antitumor activity of lithocholic acid and its derivatives. Steroids, 2017;125(June):54–60.

27. Luu TH, Bard JM, Carbonnelle D, Chaillou C, Huvelin JM, Bobin-Dubigeon C, et al. Lithocholic bile acid inhibits lipogenesis and induces apoptosis in breast cancer cells. Cell Oncol, 2018;41(1):13–24.

28. Yadav K, Bhargava P, Bansal S, Singh M, Gupta S, Sandhu G, et al. Nature of the charged head group dictates the anticancer potential of lithocholic acid-tamoxifen conjugates for breast cancer therapy. Med Chem Comm, 2015;6(5):778–87.

29. Bielenberg DR, Zetter BR. The contribution of angiogenesis to the process of metastasis. Cancer J, 2015;21(4):267–73.

30. Isik G, Kiziltay A, Hasircii N, Tezcaner A. Lithocholic Acid Conjugated mPEG-b-PCL Micelles for pH Responsive Delivery to Breast Cancer Cells. Int J Pharm, 2022;621:121779.

31. Hussein YHA, Youssry M. Polymeric micelles of biodegradable diblock copolymers: Enhanced encapsulation of hydrophobic drugs. Materials, 2018;11(5):688.

32. Moulahoum H, Ghorbanizamani F, Bayir E, Timur S, Zihnioglu F. A polyplex human saliva peptide histatin 5-grafted methoxy PEG-b-polycaprolactone polymersome for intelligent stimuli-oriented doxorubicin delivery. J Drug Deliver Sci Technol, 2022;67:102958.

33. Liao J, Peng H, Liu C, Li D, Yin Y, Lu B, et al. Dual pH-responsive-charge-reversal micelle platform for enhanced anticancer therapy. Materials Science and Engineering C, 2021;118:111527.

34. Qi P, Wu X, Liu L, Yu H, Song S. Hydrazone-containing triblock copolymeric micelles for pH-controlled drug delivery. Front Pharm, 2018;9:1–11.

35. Yang W, Soares J, Greninger P, Edelman EJ, Lightfoot H, Forbes S, et al. Genomics of Drug Sensitivity in Cancer (GDSC): A resource for therapeutic biomarker discovery in cancer cells. Nucleic Acid Res, 2013;41(D1):955–61.

36. Ferreira MJU, Gyémánt N, Madureira AM, Tanaka M, Koós K, Didziapetris R, et al. The effects of jatrophane derivatives on the reversion of MDR1- and MRP-mediated multidrug resistance in the MDA-MB-231 (HTB-26) cell line. Anticancer Res, 2005;25(6 B):4173–8.

37. Chen Y, Tang Y, Chen S, Nie D. Regulation of drug resistance by human pregnane X receptor in breast cancer. Cancer Biology and Therapy, 2009;8(13):1265–72.

38. Ciocan-Cartita CA, Jurj A, Zanoaga O, Cojocneanu R, Pop LA, Moldovan A, et al. New insights in gene expression alteration as effect of doxorubicin drug resistance in triple negative breast cancer cells. J Exp Clin Cancer Res, 2020;39(1):241.

39. Cai S, Alhowyan AAB, Yang Q, Forrest WCM, Shnayder Y, Forrest ML. Cellular uptake and internalization of hyaluronan based doxorubicin and cisplatin conjugates.pdf. J Drug Target, 2014;22(7):648–57.

40. Okur AC, Erkoc P, Kizilel S. Targeting cancer cells via tumor-homing peptide CREKA functional PEG nanoparticles. Colloids Surf B Biointerfaces, 2016;147:191–200.

41. Shin HJ, Kwon HK, Lee JH, Gui X, Achek A, Kim JH, et al. Doxorubicin-induced necrosis is mediated by poly-(ADP-ribose) polymerase 1 (PARP1) but is independent of p53. Sci Rep, 2015;5:15798.

42. Xiong H, Zhou D, Qi Y, Zhang Z, Xie Z, Chen X, et al. Doxorubicin-Loaded Carborane-Conjugated Polymeric Nanoparticles as Delivery System for Combination Cancer Therapy. Biomacromolecules, 2015;16(12):3980–8.

43. Xie X, Chen Y, Chen Z, Feng Y, Wang J, Li T, et al. Polymeric hybrid nanomicelles for cancer theranostics: an efficient and precise anticancer strategy for the codelivery of doxorubicin/ miR-34a and magnetic resonance imaging. ACS Appl Mater Interfaces, 2019;11:43865–78.

44. Mehdizadeh A, Bonyadi M, Darabi M, Rahbarghazi R, Montazersaheb S, Velaei K, et al. Common chemotherapeutic agents modulate fatty acid distribution in human hepatocellular carcinoma and colorectal cancer cells. BioImpacts, 2017;7(1):31-9.

45. Abdel-Hakeem MA, Abdel-Haseb OM, Abdel-Ghany SE, Cevik E, Sabit H. Doxorubicin loaded on chitosan-protamine nanoparticles triggers apoptosis via downregulating Bcl-2 in breast cancer cells. J Drug Deliver Sci Technol, 2020;55:101423.

46. Gao X, Yu T, Xu G, Guo G, Liu X, Hu X, et al. Enhancing the anti-glioma therapy of doxorubicin by honokiol with biodegradable self-assembling micelles through multiple evaluations. Sci Rep, 2017;7:43501.

47. Zeng X, Morgenstern R, Nyström AM. Nanoparticle-directed sub-cellular localization of doxorubicin and the sensitization breast cancer cells by circumventing GST-Mediated drug resistance. Biomaterials, 2014;35(4):1227–39.

48. Cheng X, Lv X, Xu J, Zheng Y, Wang X, Tang R. Pluronic micelles with suppressing doxorubicin efflux and detoxification for efficiently reversing breast cancer resistance. Eur J Pharm Sci, 2020;146:105275.

49. Shi J, Li J, Li J, Li R, Wu X, Gao F, et al. Synergistic breast cancer suppression efficacy of doxorubicin by combination with glycyrrhetinic acid as an angiogenesis inhibitor. Phytomedicine, 2021;81:153408.